European Journal of Pharmaceutical Sciences 211 (2025) 107132

Contents lists available at ScienceDirect

European Journal of Pharmaceutical Sciences

journal homepage: www.elsevier.com/locate/ejps

Functional enzyme delivery via surface-modified mesoporous silica nanoparticles in 3D printed nanocomposite hydrogels

Alaa Mahran [a,b], Fadak Howaili [a], Rajendra Bhadane [a,c], Rathna Mathiyalagan [a], Tapani Viitala [a], Xiaoju Wang [a,d], Jessica M. Rosenholm [a,*]

[a] Pharmaceutical Sciences Laboratory, Faculty of Science and Engineering, Åbo Akademi University, Turku 20520, Finland
[b] Department of Pharmaceutics, Faculty of Pharmacy, Assiut University, Assiut, 71526, Egypt
[c] Institute of Biomedicine, Research Unit for Infection and Immunity, University of Turku, Turku, Finland
[d] Laboratory of Natural Materials Technology, Faculty of Science and Engineering, Åbo Akademi University, Turku 20500, Finland

ARTICLE INFO

Keywords:
Cellulose nanofibers
Hydrogel extrusion 3D printing
Mesoporous silica nanoparticles
Nanocomposite biomaterial
Protein-nanoparticles interaction
MD simulation

ABSTRACT

Three-dimensional (3D) printed hydrogel-based scaffolds have emerged as promising for the delivery of biologicals. Recently, we developed a printable plant-based nanocomposite hydrogel, composed of anionic cellulose nanofibers (T-CNF) and methacrylated galactoglucomannan (GGMMA), reinforced with mesoporous silica nanoparticles (MSNs) of different surface charges. However, ensuring the biological activity of the delivered biomolecules requires further investigation to validate the functionality of the developed biomaterial. To investigate this, in this study, horseradish peroxidase (HRP) and lysozyme were selected as distinct model proteins, assessing their immobilization stability and biological activity after MSN immobilization and 3D printing. The interactions between the enzymes and differently surface-modified MSNs were explored using multi-parametric surface plasmon resonance (MP-SPR) and molecular dynamics (MD) simulations. We observed that MSN surface charge is key to the extent of enzyme adsorption and activity control. Positively charged MSNs showed the highest HRP immobilization but caused significant activity loss in both enzymes. In contrast, near-neutral and negatively charged MSNs provided improved stability and activity retention for HRP and lysozyme, respectively. Except for lysozyme/hydrogel, HRP/hydrogel and enzyme-loaded nanocomposite hydrogels (HRP-loaded near-neutral and lysozyme-loaded negatively charged MSNs) were successfully 3D printed using different UV post-curing times. While enzyme-laden nanocomposite scaffolds showed promising immobilization stability, the presence of the photoinitiator caused significant inactivation for both enzymes. Irrespective of the cross-linking approach, this matrix demonstrates significant potential as a delivery carrier for various biomolecules, with promising applications in tissue engineering and wound healing.

1. Introduction

In tissue engineering and wound healing, advanced biomaterials combined with bioactive agents, such as growth factors and enzymes, are required to enhance and regulate various biological processes of the newly developed tissues (Sufiyan et al., 2024). Among these biomaterials, hydrogel-based scaffolds have emerged as a promising platform. They support cell survival and growth by providing sufficient nutrients and essential biologicals in defective tissues. Their hydrated and porous structure offers structural similarity to the extracellular matrix (ECM) of native tissues, making them an excellent candidate for tissue engineering scaffolds (Chen et al., 2019; Vashist and Ahmad, 2015). In comparison to conventional fabrication techniques, hydrogel-based scaffolds can be constructed with high precision and fewer processing steps using the semi-solid extrusion three-dimensional (3D) printing technique (Hölzl et al., 2016; Zielińska et al., 2023). Recent advancements in 3D printing have enabled the fabrication of tailored additive-manufactured scaffolds with macroscale porous structures, suitable for integration into damaged tissues (Hassan et al., 2019). Photo-crosslinking of these 3D printed scaffolds ensures the structural integrity by exposure to UV light, which initiates a rapid crosslinking reaction that stabilizes the material effectively (GhavamiNejad et al., 2020).

Nanocellulose-based hydrogels are abundant and biocompatible

* Corresponding author.
E-mail address: jessica.rosenholm@abo.fi (J.M. Rosenholm).

https://doi.org/10.1016/j.ejps.2025.107132
Received 20 November 2024; Received in revised form 24 February 2025; Accepted 18 May 2025
Available online 18 May 2025

biomaterials with low cytotoxicity and a structure similar to the ECM, making them highly advantageous for biomedical applications (Hickey and Pelling, 2019). However, nature-derived hydrogels often require reinforcement to enhance their mechanical strength and functionality, which can be achieved by incorporating inorganic nanoparticles (Chen et al., 2019; Chakraborty et al., 2021; Soleymani Eil Bakhtiari et al., 2021; Özliseli et al., 2023). Among the various inorganic nanoparticles available, mesoporous silica nanoparticles (MSNs) have gained attention as promising carriers for bioactive agents due to their robust inorganic framework, high surface area, large pore volume, tunable pore size and customizable surface properties (Popat et al., 2011). These unique attributes make MSNs particularly effective for delivering bioactive molecules, also within hydrogel scaffolds (Castillo et al., 2020). In this regard, we recently reported semi-solid extrusion 3D printing of plant-based nanocomposite hydrogels as a protein delivery system (Mahran et al., 2023). We employed different surface-functionalized MSNs, including amino, carboxylic, and acetyl functional groups, to enhance the mechanical properties and biological activity of TEMPO-oxidized cellulose nanofibers (T-CNF). Photocurable polymer hemicellulose methacrylated galactoglucomannan (GGMMA) was used to impart photo-crosslinkable properties to T-CNF. A large-sized biological cargo (i.e., bovine serum albumin (BSA) as a model protein) was successfully delivered using MSN-laden nanocomposite biomaterial. To expand the biomedical applicability of this nanocomposite hydrogel, our aim in this study is to immobilize functional proteins to gain insights into their activity after loading and release from 3D printed nanocomposite scaffolds.

Enzymes are versatile biomolecules that catalyze essential reactions to control the process rate in living organisms such as collagenases, trypsin, and alkyl phosphatase (Holliday et al., 2009; Wang et al., 2023; Wang and Wang, 2021). Biocatalytic hydrogels have been widely fabricated and applied in tissue engineering, wound healing, and biosensing (Shen et al., 2019; Chernozem et al., 2021). In one study, researchers developed 3D printed bioactive scaffolds using alginate dialdehyde-gelatine (ADA-GEL) hydrogel augmented by lysozyme-loaded mesoporous cerium doped silica-calcia nanoparticles (Lys-Ce-MSNs). These scaffolds promoted bone regeneration while providing antioxidant and antibacterial properties (Monavari et al., 2022). However, most of the reported studies have utilized ionic crosslinking method to stabilize the 3D printed scaffolds, with limited information about the effect of the photo-crosslinking method on enzyme activity. To address this gap, enzymes are here selected as model proteins to evaluate their functionality after immobilization into our previously developed nanocomposite systems. Additionally, their catalytic activity assays offer an effective and convenient tool for detecting changes in enzyme function throughout the formulation and delivery processes.

We hypothesized that the functionality of the delivered protein could be affected by both immobilization into differently surface-charged MSNs and the 3D printing process, resulting in non-functional proteins ultimately at the target site. Thus, we developed 3D printed biocatalytic nanocomposite hydrogels by immobilizing enzymes into the previously developed nanocomposite hydrogel (Scheme 1). Additionally, we investigated the factors affecting their immobilization stability and biological activity before and after 3D printing. MSNs with different surface properties were employed to optimize the loading capacity and enzymatic activity of two model enzymes: horseradish peroxidase (HRP) and lysozyme. These enzymes differ in their molecular weights and isoelectric points (IEP) at physiological pH, which influences their interaction with various surface-charged MSNs and hydrogel components. Insights about the molecular interactions between enzymes and different charged surfaces were assessed by multi-parametric surface plasmon resonance (MP-SPR) and molecular dynamics (MD) simulations. Moreover, the rheological properties of the developed enzyme-loaded nanocomposite hydrogels were evaluated to detect their viscoelastic properties. Additionally, the impact of photo-crosslinking was evaluated after 3D printing using different UV post-curing times. Our results show successful 3D printing of the biocatalytic nanocomposite hydrogels with high enzyme immobilizing stability and promising activity retention after immobilization. However, the crosslinking method applied after 3D printing should be considered according to the mechanism of enzymatic activity. The proof-of-concept to immobilize different biological agents within the developed MSN-laden nanocomposite biomaterial was investigated, with promising application prospects for tissue engineering and wound healing.

2. Materials

Cetyltrimethylammonium chloride (CTAC) solution (25 wt % in H2O) (Milan, Italy), triethanolamine (TEA, ≥99 %) (St. Gallen, Switzerland), horseradish peroxidase (HRP) (Basel, Switzerland), tetraethyl orthosilicate (TEOS, 98 %), ammonium nitrate, glacial acetic

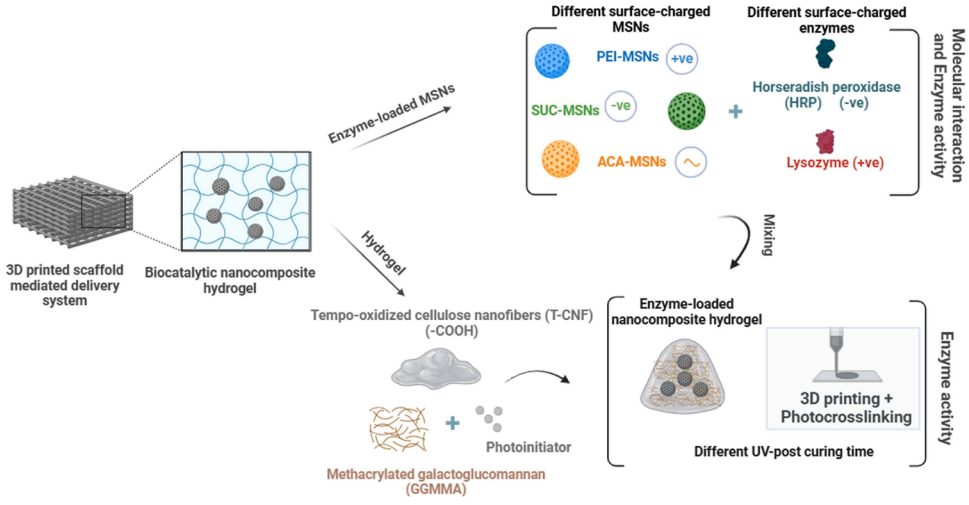

Scheme 1. Schematic illustration of the fabrication process for biocatalytic mesoporous silica nanocomposite hydrogels. Enzymes with different surface properties (Horseradish peroxidase and lysozyme) are immobilized into different surface-charged MSNs (positively, negatively, and near-neutrally charged particles), followed by analysis of the molecular interaction and measurement of enzymatic activity. Suitable enzyme-loaded MSNs are then incorporated into the hydrogel to fabricate biocatalytic nanocomposite hydrogels. Subsequently, scaffolds are fabricated using 3D printing followed by photo-crosslinking. Finally, the enzymatic activity of the released enzymes is assessed.

acid, sodium acetate, 4-(2 hydroxyethyl)−1-piperazineethanesulfonic acid buffer (HEPES), succinic anhydride (≥99 %), acetic anhydride (≥99 %), anhydrous toluene (99.8 %), cyclohexane(99.5 %), branched polyethylenimine average Mw 25,000, lithium phenyl-2,4,6-trimethylbenzoylphosphinate (LAP, ≥95 %), and Lysozyme Activity Kit (Cat. No. LY0100) were purchased from Sigma Aldrich (Steinheim, Germany). Phosphate buffer saline (pH 7.4) was obtained from Gibco (Paisley, UK). Aziridine (98 %) was obtained from Menadiona (Barcelona, Spain). TEMPO-oxidized cellulose nanofibers (T-CNF) and methacrylated galactoglucomannan (GGMMA) were in-house synthesized (using the same method described in detail in our previous work (Mahran et al., 2023)). Bradford dye reagent (Coomassie brilliant blue G-250 dye) and 1-Step™ Ultra TMB-ELISA were obtained from ThermoFisher Scientific (Rockford, USA). Lysozyme was purchased from Nordic Biosite (San Diego, USA). Double-distilled Milli-Q water was used throughout the work. All chemicals were used as received

3. Methods

3.1. Synthesis of different surface-functionalized mesoporous silica nanoparticles (MSNs)

MSNs with different surface groups, including amine (NH_2), acetyl ($COCH_3$), and carboxyl (COOH) were synthesized, aiming to generate positively, neutrally, and negatively charged surfaces, respectively. To achieve that, large pore-sized (10 nm) plain MSNs were first prepared using the biphasic method (MSNs) (Shen et al., 2014). Then, their surface silanol groups were functionalized with hyperbranched polyethylene imine through surface polymerization of aziridine (PEI-MSNs). Subsequently, the primary amino groups of PEI-MSNs were neutralized by reacting with acetic anhydride to produce near-neutrally charged nanoparticles (ACA-MSNs), while negatively charged MSNs (SUC-MSNs) were obtained by reacting with succinic anhydride. Details of the synthesis for both plain and functionalized MSNs can be found in our previous work, with no modifications to the protocol (Mahran et al., 2023).

3.2. Physicochemical characterization of the surface-functionalized MSNs

The morphological structure and mesoscopic ordering of the plain MSNs were visualized using the transmission electron microscope (TEM) (JEM 1400-Plus, JEOL Ltd., Tokyo, Japan). Malvern ZetaSizer NanoZS (Malvern Instruments Ltd., Worcestershire, UK) was used to measure the hydrodynamic diameter and ζ-potential of the synthesized nanoparticles. For dynamic light scattering (DLS) measurements, nanoparticles were suspended at a final concentration of 0.2 mg/mL in ultrapure water, while ζ-potential measurements were conducted in HEPES buffer (25 mM, pH 7.2).

3.3. Enzyme immobilization

3.3.1. Enzyme adsorption

Before immobilization, the isoelectric point (IEP) of the horseradish peroxidase (HRP) and lysozyme was determined by measuring the ζ-potential of the model enzymes in buffers with different pHs. Enzyme immobilization onto surface-functionalized MSNs was performed via the physical adsorption method. Acetate buffer (pH 5) and phosphate buffer (pH 7.4) were chosen as dispersing medium for HRP and lysozyme, respectively. First, enzymes at a concentration of 1 mg/mL and nanoparticles at 2 mg/mL were dispersed together in the buffer solutions. Then, the final dispersion was stirred gently at 25 °C for 5 h (Pota et al., 2022). Afterward, the samples were centrifuged, and the supernatants were collected to quantify the amount of unloaded enzyme. Then, the obtained solids were washed twice, and the supernatants from these washing steps were also collected to account for any remaining non-adsorbed enzyme. The enzyme-immobilized particles were then vacuum-dried. The collected supernatants (from both the initial loading solution and washing steps) were analyzed using the Bradford assay to quantify the total amount of unloaded enzyme, and the percentage adsorption capacity was calculated according to Eq. (1) (Tu et al., 2016):

$$Adsorption\ capacity\ \% = \frac{P_T - P_F}{N_T}\% \quad (1)$$

In which P_T and P_F are total protein amount and free unloaded protein amount, respectively. N_T is the total nanoparticles amount. All measurements were performed in triplicates.

3.3.2. Immobilization stability (in vitro release)

To assess the stability of enzyme-immobilized MSNs in physiological conditions, enzyme-immobilized surface-functionalized MSNs (1 mg) were suspended in 1 mL PBS buffer (pH 7.4) in a 2 mL Eppendorf tube (Chouyyok et al., 2009). The leaching experiments were carried out in the shaking water bath set to 300 rpm at 37 °C for 7 days. At specified time points (0.5, 1, 2, 4, 6, 8, 24, 48, 72, 120, 168 h), the dispersions were centrifuged at 13,000 rpm for 4 min, and 0.05 mL of clear supernatant was collected and replaced with fresh buffer. The concentration of the released enzymes was measured using the Bradford assay and quantified using UV–VIS spectroscopy. All experiments were performed in triplicates to ensure reproducibility.

3.4. Study of enzyme-MSN interaction

3.4.1. Multi-parametric surface plasmon resonance (MP-SPR)

The interaction of PEI, PEI-ACA, and PEI-SUC coated silica surfaces with model enzymes were studied at room temperature by MP-SPR Navi™ 200 instrument (BioNavis Ltd., Tampere, Finland) in 4 parallel flow channels. The peak angular position (PAP) of the reflected light at the wavelength of 785 nm was measured at the angle between 58° and 77° Silica sensor slides were used to mimic the MSN surface chemistry and were functionalized by first injecting a PEI solution with a concentration of 0.2 mg/mL to achieve a positively charged surface. To render the silica sensor surface negatively or near-neutral charged, then PEI along with SUC or ACA at a concentration of 0.4 mg/mL diluted in EtOH, was injected to coat the silica sensor surface, respectively. HRP and lysozyme were dissolved in acetate buffer (pH 5) and PBS (pH 7.4), at a concentration of 50 μg/mL. The injection orders for all buffers used in HRP and Lysozyme experiments are shown in **Tables S1 and S2**, respectively. The interaction of the silica sensor with PEI, PEI-SUC, and PEI-ACA coatings are presented as MP-SPR sensograms in **Fig. S1**. Measurements were conducted at a flow rate of 30 μL/min for approximately 10 min for each injection. The SPR response data was extracted by using the SPR Navi Data viewer software (version 6.7.0.9, Bionavis Ltd, Tampere, Finland). The injection start point was set as zero when the enzymes were injected. The kinetic parameters were determined in TraceDrawer (version 1.7) modeling software by fitting the SPR sensograms with One-To-One Langmuir model (Souto et al., 2015). Additional data analysis was performed with GraphPad Prism (version 8.0.2, San Diego, CA).

3.4.2. Molecular dynamic (MD) simulation

To obtain representative models of MSNs under investigation and to understand MSN–protein interactions at the interface, atomic scale models of PEI, ACA, and SUC-modified MSNs were prepared ignoring the noninteracting core of nanoparticles. The structures of these functionally modified silica surfaces were sketched using 3D builder panel of maestro (Schrödinger, LLC, New York, NY, 2023). The 3D structure of HRP and Hen Egg White Lysozyme (PDB ID:1H57 and 1DPX (Berglund et al., 2002), (Weiss, Palm, and Hilgenfeld 2000), respectively) were imported from the protein data bank (PDB) (Berman et al., 2000). The protein structure was imported and processed using a protein preparation workflow. Briefly, bond orders and hydrogen bond assignments were carried out. This is followed by generating het states with Epik at

pH 7.0 ± 2.0 (Shelley et al., 2007). In the next step, assigned hydrogen bonds were optimized using PROPKA at a neutral pH (Søndergaard et al., 2011; Olsson et al., 2011). In the final step, the structures were briefly minimized using the OPLS4 force field (Lu et al., 2021) with a 0.30 Å root-mean-square deviation (RMSD) of the heavy atom displacement as a convergence criterion. The water molecules further than 3 Å from the ligand were deleted. To prepare a simulation system with a set number of polymers and protein molecules, the Disordered System Builder panel of the Schrödinger Material Science suite (Schrödinger, LLC, New York, NY, 2023) was used. The maximum number of protein molecules in each system was 1. Each system had an initial density of 0.5 g/cm^3 and periodic boundary conditions (PBC) with an orthorhombic unit cell were used for all simulations. The initial disordered system was set to a "amorphous" using the OPLS4 force field.

The PEI, ACA, and SUC-modified MSNs with HRP and Lysozyme were submitted to a 100-ns molecular dynamics (MD) simulation. The simulation was performed using the multistage MD simulation workflow of Desmond (Schrödinger Release 2023: Desmond Molecular Dynamics System, D. E. Shaw Research, New York, NY, USA, 2023; Maestro-Desmond Interoperability Tools, Schrödinger, New York, NY, USA, 2023) (Bowers et al., 2008), consisting of a three-stage material relaxation protocol, followed by the production MD simulation and analysis. Briefly, the material relaxation protocol involved 20 ps of Brownian dynamics (BD) at 10 K to remove steric clashes, followed by a short BD simulation at 100 K in the NPT ensemble and an anisotropic coupling scheme. In the final stage, a 100-ps MD simulation in the NPT ensemble was completed using anisotropic coupling and a 2-fs time step. The production simulation was then performed for 100 ns at 300 K and 1.01325 bar with the Nose-Hoover chain thermostat (Braga and Travis, 2005; Hoover, 1985) and barostat using the Martyna-Tobias-Klein method with isotropic coupling (Martyna et al., 1999). The Coulombic method used for long-range interactions was U-series while the cut-off radius for short-range interactions was set to 9.0 Å (Predescu et al., 2020). The interactions between MSN surface and protein molecules were calculated from the simulation trajectories and were further analyzed in Microsoft Excel365.

3.4.3. ζ-potential of enzyme-immobilized MSNs

The ζ-potential of enzyme-immobilized MSNs was measured to investigate the impact of protein adsorption on the surface charge of the particles. These measurements were performed under the same conditions described in Section 3.2.

3.5. Biological activity of immobilized and free-released enzymes (specific activity and residual activity)

The biological activity of the immobilized and free-released enzymes was evaluated to study the effect of the immobilization process on enzymatic activity. Further, the best formulation for both enzymes was used for nanocomposite preparation.

The catalytic activity of HRP was assessed calorimetrically using 3,3′,5,5′ tetramethylbenzidine (TMB) (Lin et al., 2011). TMB is a chromogenic substrate that produces a blue-colored product upon oxidation by hydrogen peroxide with a reaction catalyzed by HRP. The color then changes to yellow upon the addition of sulfuric acid. Briefly, 0.2 mg of HRP-loaded functionalized MSNs were redispersed in 0.3 mL PBS buffer pH 7.4. Then, the suspended particles were mixed with 1.5 mL TMB Elisa solution and waited for a given period. The reaction was terminated using 1.5 mL of 2 M sulfuric acid, and the formed colored product was measured by UV–Vis spectroscopy at 450 nm. All samples were measured in triplicates.

HRP enzymatic activity in (Units/mL) is defined as the amount of TMB (μmoles) transformed per minute (μmol min^{-1}). The enzyme activity was calculated using Eq. (2)

$$HRP\ enzymatic\ activity\ (Units/mL) = \frac{(\Delta - \Delta_B) \times total\ volume\ of\ the\ reaction}{\varepsilon_{TMB} \times P \times sample\ volume} \quad (2)$$

Where, Δ and Δ_B are the absorbance of the tested sample and blank, P is the optical path in cm, which is 1 for cuvettes and 0.58 in a 96-well plate when the reaction volume is 200 μL, and Ɛ is the molar extinction of oxidized TMB at 450, ($Ɛ_{TMB}$= 59,000 $mol^{-1}cm^{-1}$).

Lysozyme catalytic activity was measured based on a continuous reading of the change in the turbidity of a bacterial suspension upon lysis. Lysozyme is a bacteriolytic enzyme that hydrolyzes the peptidoglycan layer of bacterial cell walls, thereby decreasing the turbidity of the suspension (Dyawanapelly et al., 2019). The catalytic activity of immobilized lysozyme was measured according to Sigma Aldrich instructions: 0.2 mg of lysozyme-loaded functionalized MSNs were redispersed in 0.1 mL reaction buffer (66 mM KH_2PO_4, pH 6.2). Then, 2.5 mL of freshly prepared Micrococcus lysodeikticus cell suspension in reaction buffer was added. The change in the optical density of cell suspension was recorded every 1 min and over 5 min period at 450 nm using UV–VIS spectroscopy. All measurements were conducted in triplicates

Lysozyme enzymatic activity in (Units/mL) is defined as the amount of enzyme that produces a ΔA_{450} of 0.001 per minute at pH 6.24 at 25 °C using a suspension of Micrococcus lysodeikticus as substrate, in a 2.6 mL reaction mixture (1 cm pathlength) and calculated using Eq. (3):

$$Lysozyme\ enzymatic\ activity\ (Units/mL) = \frac{(\Delta A_{450}/\mathrm{min}test - \Delta A_{450}/\mathrm{min}Blank) \times df}{(0.001)(0.03)} \quad (3)$$

Where d_f is the dilution factor, 0.001 is the ΔA_{450} as per the unit definition and 0.03 is the volume (in milliliters) of enzyme solution.

Specific activity is defined as the enzymatic activity per mg of protein (Units/mg) and calculated for both enzymes using Eq. (4) (Weishaupt et al., 2015)

$$Specific\ activity\ (Units/mg) = \frac{enzyme\ activity\ \left(\frac{units}{mL}\right)}{\frac{mass\ of\ solid\ (mg)}{volume\ of\ enzyme\ (mL)}} \quad (4)$$

The residual activity of the free-released HRP and lysozyme was quantified from an aliquot containing the released enzymes at two different time points (24 h and 7 days). The calibration curve was

constructed based on known enzyme concentration using a 96-well plate (**Fig. S2**) (supplementary method for more detailed description). Then, the activity was calculated using Eq. (5)

$$Residual\ activity\ \% = \frac{enzyme\ activity\ after\ release\ \left(\frac{Units}{mL}\right)}{actual\ enzyme\ activity\ \left(\frac{Units}{mL}\right)} \quad (5)$$

3.6. Printing of the enzyme-loaded mesoporous silica nanocomposite hydrogel

3.6.1. Nanocomposite hydrogel preparation

The nanocomposite hydrogels were prepared by physical incorporation of HRP-loaded ACA-MSNs and lysozyme-loaded SUC-MSNs (1 wt %) into a prewarmed hydrogel at 50 °C. The hydrogel was prepared using 1 wt % T-CNF as the main hydrogel matrix, 3 wt % GGMMA as the photocurable polymer, and 0.2 wt % LAP as the photointiator. The concentration of enzyme-loaded MSNs was chosen based on our previous study. To compare the performance of enzymes without MSNs, 0.1 wt % free enzymes (HRP and lysozyme) were mixed with the plain hydrogel. All prepared hydrogels were centrifuged at 3000 rpm for 5 min to remove air bubbles.

3.6.2. Rheological assessment of the nanocomposite hydrogels

Rheological properties of the enzyme-loaded hydrogels and enzyme-loaded nanocomposite hydrogels were evaluated and compared with plain hydrogel to gain information about their flow behavior and viscoelastic properties. The HAAKE MARS Modular Advanced Rheometer system (Thermo Scientific, Karlsruhe, Germany) with a 20 mm diameter cone-plate geometry (1° cone angle with a truncation gap of 0.049 mm) was used in all measurements, and the temperature was set at 23 °C. All samples were equilibrated before each measurement at a shear rate of 0 s^{-1} for 60 s. The flow behavior was evaluated using a shear rate ramp-up of 0.01–1000 s^{-1} in a logarithmic scale with 1 s per data point. From the power law equation, the consistency index was calculated using Eq. (6)

$$\eta = k\dot{\gamma}^{n-1} \quad (6)$$

where η is the dynamic viscosity, $\dot{\gamma}$ is the shear rate, K is the consistency index, and n is the power law index.

The amplitude sweep test was conducted to determine the viscoelastic properties of the prepared hydrogels. It was performed by applying a shear strain from 0.0 % to 10 % at a constant frequency of 1.6 Hz with a data acquisition time of 10 s per data point. Three parameters were obtained from the amplitude sweep test: linear viscoelastic region (LVER), gel strength, and flow transition index (FTI). LVER is the shear strain value at which shear stress deviates from linearity by 10 %. Gel strength is the storage modulus value (G') at the end of LVER. Finally, Eq. (7) was used to calculate the FTI

$$FTI = \frac{\tau_f}{\tau_y} \quad (7)$$

where τ_f and τ_y represent the flow stress and yield stress, respectively. Flow stress is the shear stress value at the crossover point between storage modulus (G') and loss modulus (G''), whereas yield stress is the shear stress value at the end of the LVER.

3.7. Printing of the nanocomposite hydrogel

Enzymes-loaded hydrogels and enzyme-loaded nanocomposite hydrogels were 3D printed using extrusion-based 3D printing (Brinter One, Brinter AM Technologies Ltd, Finland). The small inner diameter (0.25 mm) stainless steel needles (Nordson EFD, USA) were used for the plain hydrogel and enzyme-loaded hydrogel. In contrast, the larger inner diameter (0.33 mm) was used for printing nanocomposite inks to reduce repeated nozzle clogging caused by nanoparticles. The print bed and pneumatic tool-cooled printhead were maintained throughout the study at 16 °C and 20 °C, respectively. A four-layered grid construct was printed at a speed of 10 mm s^{-1} and a pressure of 350 ± 20 mbar. Photocrosslinking was done using a UV/Vis LED module with wavelength 405 nm and intensity of 17.5 mW cm^{-2} for 30 s after each layer. Additionally, three different UV post-curing times (1, 5, and 10 min) were applied to assess the effect of curing time on enzyme release and biological activity.

3.7.1. Immobilization stability and enzymatic activity after 3D printing

The immobilization stability of the final constructs was evaluated by weighing the 3D printed scaffolds followed by suspending them in 1 mL PBS buffer and continuously stirring for 7 days using the same settings listed in Section 3.3.2.

Subsequently, the enzymatic residual activity after release from the 3D printed scaffolds and after mixing with the hydrogel components (T-CNF, GGMMA, and the photointiator LAP) was measured following the same protocol stated in Section 3.5.

3.8. Statistical analysis

Statistical analyses were performed using GraphPad Prism version (8.0.0). One-way ANOVA followed by Tukey post-hoc test were used to analyze the differences between experimental groups. Two-tailed, unpaired student's *t*-test was carried out to analyze the significance between two groups. The differences were considered significant at $p \leq 0.05$.

4. Results and discussion

4.1. Synthesis and characterizations of differently surface-functionalized MSNs

Mesoporous silica nanoparticles (MSNs) with different surface modifications were synthesized to elucidate the role of surface functional groups on enzyme adsorption and biological activity. Large pore-sized MSNs of approximately 10 nm were synthesized using the biphasic method (Shen et al., 2014). The morphology of the plain MSNs was visualized by TEM, which revealed a uniform spherical shape and a highly porous dendritic structure (Fig. 1**A**).

The surface silanol groups of plain MSNs on one hand imparts an overall negative net surface charge to non-modified particles; and on the other hand, also play a crucial role as anchoring points allowing surface functionalization and thus modification of the surface properties. Fig. 1**B** shows a schematic illustration of the applied methods to achieve differently surface-functionalized MSNs. Although various approaches can be used to introduce surface amino groups, surface hyperbranching polymerization of aziridine is the most efficient method due to its ability to provide a high yield of terminal primary amino groups owing to the hyperbranched mode of growth (PEI-MSNs) (Rosenholm and Lindén, 2007). The subsequent reaction of PEI-MSNs with acetic anhydride results in a near-neutral net (overall) surface charge by capping the primary amino groups of PEI with non-charged acetyl groups (ACA-MSNs). The remaining charges originates from a competition between the remaining secondary and tertiary amino groups of the PEI layer and unreacted silanol groups of the MSN itself (Karaman et al., 2012). Further reaction of PEI-MSNs with succinic anhydride introduces negatively charged carboxylic acid terminal groups on the surface (SUC-MSNs).

Table 1 summarizes the physicochemical properties of the synthesized nanoparticles. All particles showed small hydrodynamic diameters of less than 300 nm with a small PDI value of less than 0.2, indicating full aqueous dispersibility of the prepared particles. Successful surface modifications were confirmed by measuring the ζ-potential of the prepared particles at neutral pH (HEPES buffer, pH 7.2). Plain MSNs with a

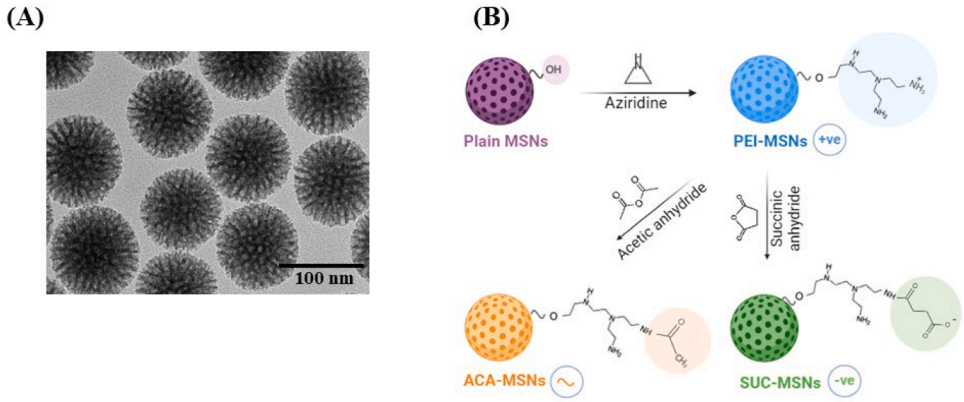

Fig. 1. (A) Transmission electron microscopy (TEM) image of plain MSNs. (B) Detailed illustration of different surface-functionalized MSNs. First, plain MSNs were reacted with aziridine to yield hyperbranched polyethyleneimine branches on the surface (PEI-MSNs). Further, PEI-MSNs were reacted with acetic anhydride to yield near-neutral nanoparticles (ACA-MSNs) and succinic anhydride to obtain negatively charged nanoparticles (SUC-MSNs).

Table 1
Physicochemical characterization of the prepared particles. Ultrapure water was used for dynamic light scattering (DLS) measurements and HEPES buffer (pH 7.2, 25 mM) for ζ-potential measurements.

Sample name	Hydrodynamic diameter (nm)	Polydispersity index (PDI)	ζ -Potential (mV)
Plain MSNs	134.5 ± 0.4	0.114	- 28.8 ± 1.4
PEI-MSNs	148.0 ± 1.5	0.023	+ 41.6 ± 1.5
ACA-MSNs	160.0 ± 2.0	0.121	- 14.3 ± 0.6
SUC-MSNs	245.0 ± 0.1	0.134	- 36.1 ± 2.0

negative net surface charge (−28.8 mV) were shifted to a high net positive surface charge (+41 mV) after reaction with aziridine (PEI-MSNs). Near-neutral ζ-potential (−14 mV) was obtained for ACA-MSNs, while a negative ζ-potential was measured for SUC-MSNs (−36 mV) under the studied conditions.

4.1.1. Enzyme immobilization

Generally, the large surface area of bare MSNs provides a high adsorption capacity for different biologicals, which can be either adsorbed onto the particle surface or inside the pores on the pore walls. In this context, pore size is the main determinant, affecting protein loading and leaching (Yiu and Wright, 2005; Zhou and Hartmann, 2013). However, introducing different surface functional groups to bare MSNs alters the adsorption properties of the particles, influenced by the nature and surface charge of the added groups. Therefore, we investigated the effect of different surface modifications on the adsorption and leaching of two distinct model enzymes: horseradish peroxidase (HRP) and lysozyme (see **Table S3)**. HRP is a relatively large enzyme with a hydrodynamic diameter of ~ 6.0 nm and a molecular weight of 35–40 kDa. It is a heme-containing enzyme, which uses hydrogen peroxide to oxidize different organic and inorganic compounds (Veitch, 2004; Pandey et al., 2017). In contrast, lysozyme is a small-sized enzyme with a hydrodynamic diameter of ~3.8 nm and a molecular weight of 14 kDa. It is an anti-bacterial enzyme, which hydrolyzes the peptidoglycan layer of the bacterial cell walls (Merlini and Bellotti, 2005). From the literature, HRP has a net negative surface charge at neutral pH while lysozyme exhibits a net positive surface charge at physiological conditions (Rahmatika et al., 2019). For both enzymes, the adsorption capacity and immobilization stability were determined. The interaction between unfunctionalized MSNs with HRP and lysozyme has been well studied in previous research, considering several parameters such as pore size and shape as well as particle shape (Lin et al., 2011; Chouyyok et al., 2009), (Kao et al., 2014; Wang et al., 2016; Xiao et al., 2008); therefore, our focus was on the surface-modified MSNs, using plain MSNs data as a reference.

4.1.2. Enzyme adsorption

The adsorption conditions for the model enzymes were optimized based on their isoelectric points (IEP), which represent the pH at which protein loading is most favorable (Miyahara et al., 2006). Namely, at this pH, electrostatic repulsion between protein molecules is minimized, allowing them to pack more closely on the silica surface than at any

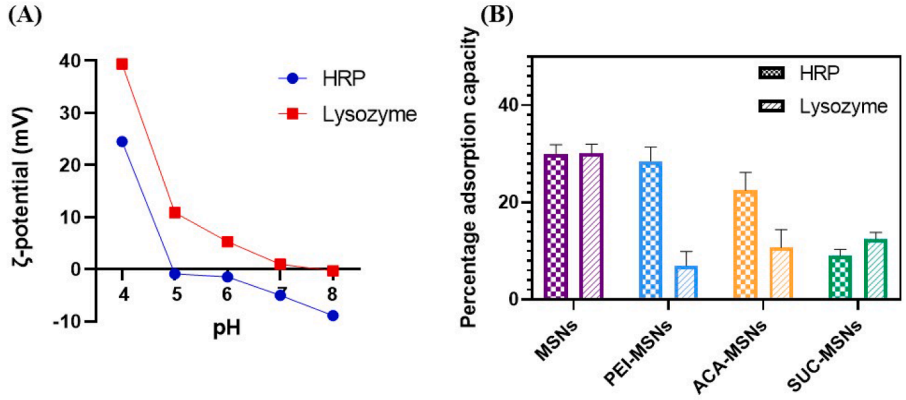

Fig. 2. (A) The pH dependency of the ζ-potential of HRP and lysozyme, illustrating their isoelectric points (IEP) at 0 mV. (B) The adsorption capacity in percent of the immobilized enzymes (HRP and lysozyme) onto functionalized and unfunctionalized MSNs after 5 h using acetate buffer pH 5 for HRP and phosphate buffer pH 7.4 for lysozyme as loading solutions.

other pH (Su et al., 2000). Although the protein surface may exhibit a complex charge distribution at pH equal to its IEP, the overall net charge remains zero (Sang et al., 2011). Based on zeta potential measurements across different pH values, HRP was thus immobilized using acetate buffer (pH 5), and lysozyme was immobilized using phosphate buffer (pH 7.4) (Fig. 2**A**). HRP and lysozyme were adsorbed onto different surface-functionalized MSNs at the specified pH, and Fig. 2**B** represents the percentage adsorption capacity of both enzymes.

Compared to surface functionalized particles, plain MSNs showed the highest adsorption capacity of both enzymes, with no significant difference in their adsorption percentage (around 30 %). Using large pore-sized MSNs (10 nm) effectively excluded the impact of pore size, as confirmed by the similar immobilization percentage. Apart from particle surface charge, HRP exhibited greater immobilization onto surface-modified particles than lysozyme, likely due to the difference in their sizes. The large size of HRP may provide more active points for interaction, leading to enhanced immobilization. These active sites might involve more electrostatic, hydrogen bonding, and van der Waals interactions (Wang and Caruso, 2005).

The immobilization efficiency of HRP varied significantly depending on the net surface charge of the MSNs. PEI-MSNs (positively charged) exhibited the highest enzyme immobilization (28.5 %), which was significantly higher than that observed for near-neutral MSNs (ACA-MSNs: 22.5 %, $p < 0.01$) and negatively charged MSNs (SUC-MSNs: 9 %, $p < 0.0001$). In contrast, negatively charged particles (SUC-MSNs) showed the highest lysozyme immobilization efficiency (12 %), followed by ACA-MSNs (10 %) and PEI-MSNs (6 %). SUC-MSNs and ACA-MSNs exhibited no significant difference in immobilization efficiency, but both demonstrated significantly higher immobilization than PEI-MSNs ($p < 0.01$). The change in the adsorption order is mainly correlated to the effect of adsorption pH on the surface properties of the enzyme and particle during immobilization. HRP immobilization was carried out at pH 5. At this pH, all particles exhibited a net positive surface charge with a higher value observed for PEI-MSNs (**Fig. S3**), while HRP displayed a slight net negative surface charge. On the other hand, lysozyme immobilization was performed at pH 7.4. At this pH, only SUC-MSNs and ACA-MSNs showed a net negative surface charge with high negativity observed for SUC-MSNs (Table 1), while lysozyme carries a slightly net positive surface charge. These electrostatic attractive and repulsive forces between the enzymes and functionalized MSNs are the main driving force of more HRP and lysozyme adsorption onto PEI-MSNs and SUC-MSNs, respectively. Regarding near-neutral MSNs (ACA-MSNs), both enzymes were immobilized without any preference for the surface charge of the enzyme compared to positively and negatively charged particles. This might be attributed to, at the adsorption pH for both enzymes, ACA-MSNs exhibited surface charges opposite to that of the loaded enzymes but with less charge density than PEI-MSNs and SUC-MSNs, which enhances their interaction with both enzymes. Under these experimental conditions, enzyme size and the surface properties of both enzymes and nanoparticles are the dominant drivers for protein adsorption.

4.2. Immobilization stability (in vitro release)

The immobilization stability test was carried out to evaluate the strength of interaction between enzymes and different surface-functionalized MSNs at physiological pH. Fig. 3 compares the cumulative release profile of both enzymes. For plain MSNs, less than 5 % of the adsorbed HRP was released after 8 h, while less than 17 % of the adsorbed lysozyme was released after 4 h. Additionally, the maximal release percentage of lysozyme across all particles was higher and reached faster than HRP. This indicates an inverse correlation between the final release percentage and the molecular size of the enzyme. The results confirm that lysozyme has a weaker interaction with the particles compared to HRP, which is consistent with the enzyme adsorption data.

Fig. 3**A** shows that the cumulative release percentage of HRP was higher from neutral and negatively charged particles than from positively charged particles. The maximum release percentage from ACA-MSNs and SUC-MSNs was nearly the same (22 %). However, it was reached faster for ACA-MSNs (22 % after 2 h) than for SUC-MSNs (22 % after 24 h). On the other hand, PEI-MSNs showed a maximum release of only 10 % after 24 h, probably due to the strong interaction between PEI-MSNs and HRP. A probable explanation of the different release patterns between the formulations is the effect of pH on enzyme adsorption and desorption, mainly its effect on the electrostatic interactions (Lin et al., 2011; Vinu et al., 2004). The shift from the adsorption pH 5 (acidic pH) to leaching pH 7.4 (neutral pH) caused a change in the net surface charge of the nanoparticles and the adsorbed HRP except PEI-MSNs. At the leaching pH, the surface charge of ACA-MSNs and SUC-MSNs shifted from a positive to a neutral or negative net surface charge, while the HRP surface exhibited more negative surface potential. This resulted in a decrease in the electrostatic attraction forces and greater release compared to PEI-MSNs, which showed no change in the net surface charge.

Fig. 3**B** shows that lysozyme exhibited almost the same maximum release percentage (50 %) from all particles (PEI-MSNs, ACA-MSNs, and SUC-MSNs). However, SUC-MSNs reached a maximum release after 2 h, while PEI-MSNs and ACA-MSNs achieved maximum release after 4 h. This further confirms the role of pH and weak adsorption of lysozyme. The adsorption strength and different types of interactions involved between enzymes and charged MSNs will be discussed in detail in the next section.

4.3. Enzyme-MSN interactions

Investigating the interactions between functional proteins (e.g., enzymes) and different surface-charged nanoparticles is essential to assessing the potential impact of the nanoparticle environment on the biological activity of these proteins. Different approaches can be used to study protein and protein adsorption onto surfaces (Kubiak-Ossowska et al., 2019). Combining experimental and computational approaches will give more insights about protein adsorption from different perspectives. Hence, we used two complementary methods to gain more

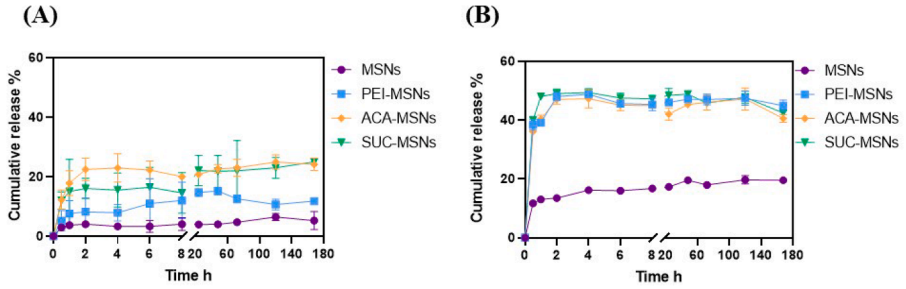

Fig. 3. Immobilization stability study, cumulative release profile of (A) HRP and (B) lysozyme from functionalized and unfunctionalized MSNs using PBS buffer pH 7.4 and at 37 °C for 7 days.

information about enzyme adsorption and interaction with differently charged MSNs: multi-parametric surface plasmon resonance (MP-SPR) and molecular dynamics (MD) simulations. The impact of protein adsorption on the net surface charge of the nanoparticles was also studied by measuring the ζ-potential of the enzyme-loaded MSNs.

4.4. Multi-parametric surface plasmon resonance (MP-SPR)

The MP-SPR sensogram provides a comprehensive understanding about interaction kinetics and affinity for the interaction between enzymes and the silica sensor surface. The sensogram typically consists of distinct phases including the association phase (where the enzyme binds to sensor), equilibrium (steady state binding), and the disassociation phase (where the enzymes detach from the sensor). The shape of the sensogram allows quantification of the kinetic interaction parameters. The kinetic parameters derived from fitting the SPR sensograms using a One-To-One model provide deeper insight for the binding dynamics. The maximum response (mRU) when the sensor surface is fully occupied by the enzymes is represented by B_{max}, while the association rate constants (k_a) evaluate how fast the enzyme binds to the silica sensor and functionalized silica sensor, whereas the disassociation rate constant (k_d) determines how fast the enzyme disassociates. The last parameter, the equilibrium dissociation constants (K_D=k_d/k_a) indicate the binding affinity, in other words, how tightly the enzyme binds to the silica sensor and functionalized silica sensor (Koretz et al., 2021). The lower the K_D value, the stronger the affinity between the enzyme and the functionalized surface.

In this research, the interaction of HRP and lysozyme with a silica sensor functionalized with different coatings using MP-SPR was conducted to evaluate the binding kinetics and affinity. The successful functionalization of the silica sensor with PEI, PEI-ACA, and PEI-SUC was confirmed by the shift in the SPR signal, as shown in the sensogram (**Fig. S1).** The interactions of HRP and lysozyme with the silica sensor and the functionalized silica surfaces are shown in Fig. 4 illustrating the interaction intensity trends of HRP and lysozyme with each coating.

When comparing the MP-SPR responses for HRP binding to the different functionalized silica surfaces, then the largest SPR angular shift was observed for HRP binding to both unmodified silica sensor and Si-PEI, whereas the Si-PEI-ACA and Si-PEI-SUC coatings showed lower and relatively similar SPR angular shifts. The difference in the intensity of HRP interacting with different surface modifications can be attributed to variations in the interaction at the corresponding pH, as it is discussed in enzyme adsorption section (Fig. 4**A)**. The sensograms of the interaction of HRP with different silica surface modifications were fitted to a One-To-One model. As it is shown in Table 2**,** there is no significant difference in the K_D values between Si-HRP and Si-PEI-HRP samples, nor between Si-PEI-ACA-HRP and Si-PEI-SUC—HRP. However, the comparison of the k_a and k_d values suggests that HRP associates more rapidly with Si-PEI-ACA and Si-PEI-SUC surfaces, while dissociating more slowly from these surfaces compared to others. Therefore, HRP has slightly higher affinity to Si-PEI-ACA and Si-PEI-SUC surfaces. This indicate that affinity alone does not fully account for the sensogram intensity ranking of HRP interactions with different modifications. However, the B_{max} values, which show the maximum response for each modification, align with the sensogram intensities and the adsorption capacity described in the Section 4.2.1 for the three surface modifications.

Table 2
Kinetic parameters of HRP interaction with silica sensors and silica sensors having different surface functionalizations.

Sample name	B_{max}(mRU)	k_a (M^{-1} s^{-1})	k_d (Sec^{-1})	K_D(M)
Si-HRP	201.52 (±7,45E-2)	1,92E+3 (±1,98E+2)	7,36E-4 (±5,15E-6)	3,38E-7 (±4,27E-8)
Si- PEI-HRP	235.08 (±2,00E-1)	1,78E+3 (±3,92E+2)	7,92E-4 (±1,98E-5)	4,44E-7 (±1,14E-7)
Si-PEI-ACA-HRP	148,22 (±2,14E-1)	2,06E+3 (±3,72E+3)	2,18E-4 (±1,71E-5)	1,06E-7 (±8,85E-8)
Si-PEI-SUC—HRP	139,69 (±1,22E-1)	2,37E+3 (±5,10E+2)	4,48E-4 (±9,69E-6)	2,04E-7 (±5,02E-8)

Regarding lysozyme, the sensogram of lysozyme interacting with the silica sensor and its functionalized coatings could not be fitted to the One-To-One due to the absence of a distinct dissociation phase. As a result, the k_d could not be determined, making it impossible to calculate the K_D value. However, MP-SPR responses suggest that the strongest binding occurs between unmodified silica and lysozyme. Additionally, the sensograms shows relatively similar binding response for Si-PEI-ACA and Si-PEI-SUC compared to Si-PEI (Fig. 4**B**).

To conclude, the differences in binding patterns and response levels between HRP and lysozyme, observed from the SPR signal, are likely due to enzyme-specific interactions with corresponding coating. This suggests that lysozyme exhibits weaker binding interactions than HRP, primarily due to its smaller size and fewer active binding sites **(**see Fig. 2 **and Table S3)** (Wang and Caruso, 2005; Lin et al., 2011**)**.

4.4.1. Molecular dynamics simulations

To date, many protein-nanoparticle formulations have been reported in the literature (Huang et al., 2018; Deere et al., 2002; Rezwan et al., 2005) but most of these formulations were unable to provide molecular insights into the interactions between the protein molecules and the nanoparticles. Hence, we performed MD simulations of each MSN system with HRP and lysozyme. While preparing the system of this size at atomic scale, where protein molecules need to be surrounded by few MSN particles, is computationally demanding and complicated. As our aim is to investigate the effect of surface functionalization of MSNs on these two protein molecules, we used small silica chains and performed PEI modification on them. These PEI-modified MSNs were further modified to get ACA and SUC modified MSNs for this study. We predicted the charge distribution of the protein surface and how it affects the interaction pattern with different MSNs. We further detailed the variation in the interactions with different functional modifications of MSN and how these interactions could affect the functional properties of

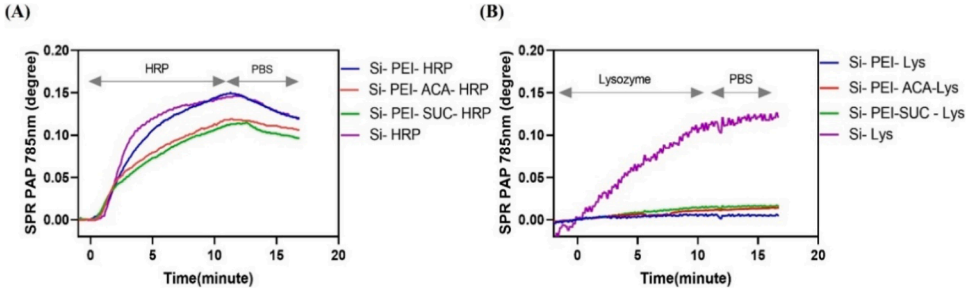

Fig. 4. MP-SPR response during the interaction of enzymes (A) HRP and (B) lysozyme with silica sensors and silica sensors functionalized with the same functional groups as the studied MSNs.

the enzymes under investigation.

It is well known that physical adsorption is considered the simplest method of immobilization in which an enzyme is immobilized onto a carrier and the biocatalysts are held on the surface of the carriers by different physical forces including van der Waals, hydrophobic interactions, hydrogen bonding, and ionic interactions. These interactions have a great impact not only on the stability of the immobilized enzyme but also on its activity. The MD simulations employed in this study investigated the molecular interactions between different surface-functionalized MSNs and HRP and lysozymes, exhibiting different surface properties giving an overall view of the enzyme adsorption and its functions.

As compared to surface functionalized MSNs, which show more uniformity in charge distribution over their surface, the charge distribution on the surface of the protein is much more complex and it largely depends on the orientation of amino acids. **Fig. S4** shows electrostatic charge distribution on the surface of the protein before simulation. These surface orientations of amino acids are dynamic in nature and often change with respect to surroundings. When we performed MD simulation of these protein molecules with functionalized MSNs, we observed the changes in protein conformation as per the type of functionalized MSNs involved in the interaction with the protein. Apart from surface interactions, we observed the involvement of specific amino acids in enzyme catalysis, and their interactions with functionalized MSNs have a profound effect on the activity of the enzyme (see the next section). Overall, the bigger changes in the protein conformation and its activity were observed with PEI-MSNs followed by SUC-MSNs and the least effect of ACA-MSNs. To provide detailed insights about all these interactions, we compared interactions with different functionalized MSNs with HRP and lysozyme.

It was observed that PEI-modified MSNs form hydrogen bonding interactions with both HRP and lysozyme with small differences in the number of these interactions (see Figs. 5 **and** 6). It is worth mentioning that electrostatic interactions through salt bridges were observed with both enzymes. However, these interactions are significantly higher with HRP as compared to lysozyme. Apart from hydrogen bonding and electrostatic interactions, PEI-MSNs also show van der Waals and π-cation interactions. The π-cation interactions are unique for PEI-MSNs as they originate from the interaction of positively charged cations and negatively charged electron clouds of the π system. Overall, the interaction of PEI-MSNs with HRP is quite significant compared to lysozyme.

On the other hand, the interaction magnitude of SUC-MSNs with

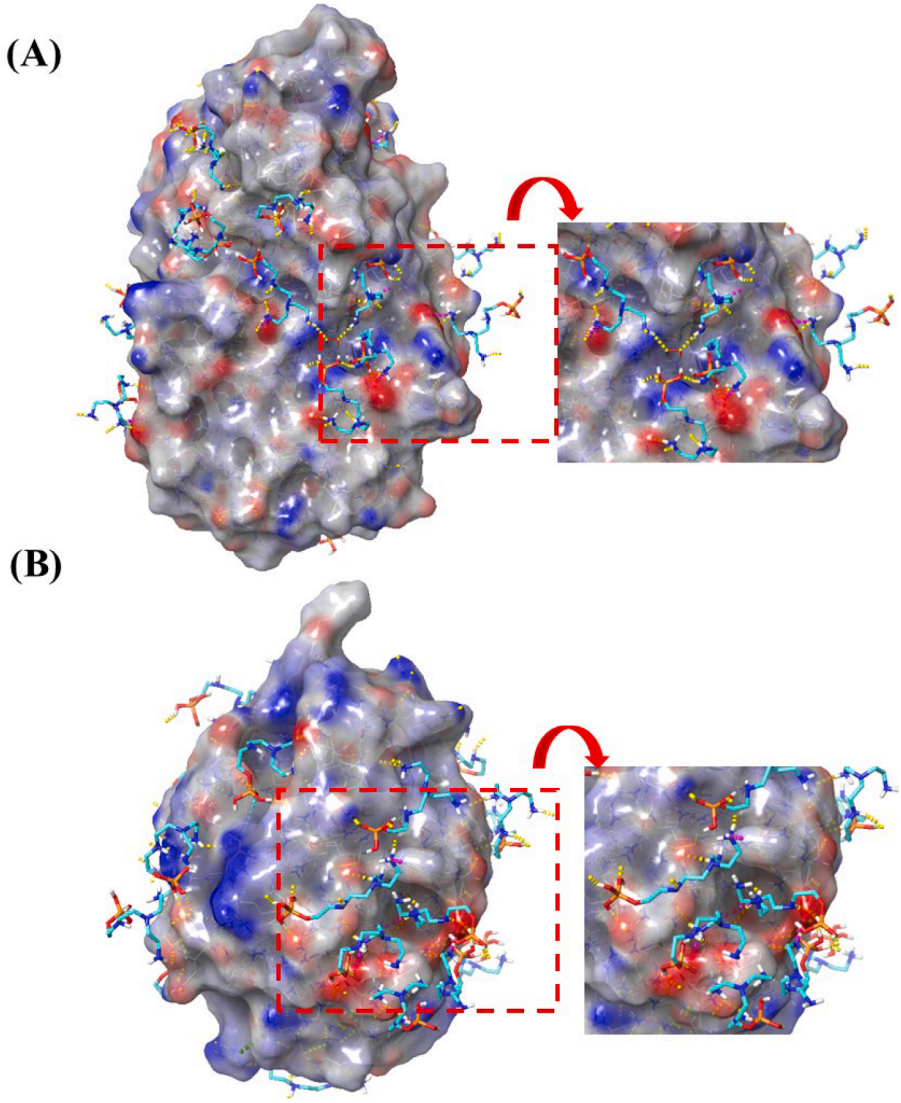

Fig. 5. (A) Electrostatic surface view of HRP showing charge distribution after 100 ns MD simulation with PEI-MSNs; (B) Electrostatic surface view of lysozyme showing charge distribution after 100 ns MD simulation with PEI-MSNs. Color scheme: basic amino acids: blue, acidic amino acids: red, PEI-MSNs: cyan color sticks, hydrogen bonds: yellow, salt bridges: pink, π-cation: green, aromatic hydrogen bonds: cyan color dash lines.

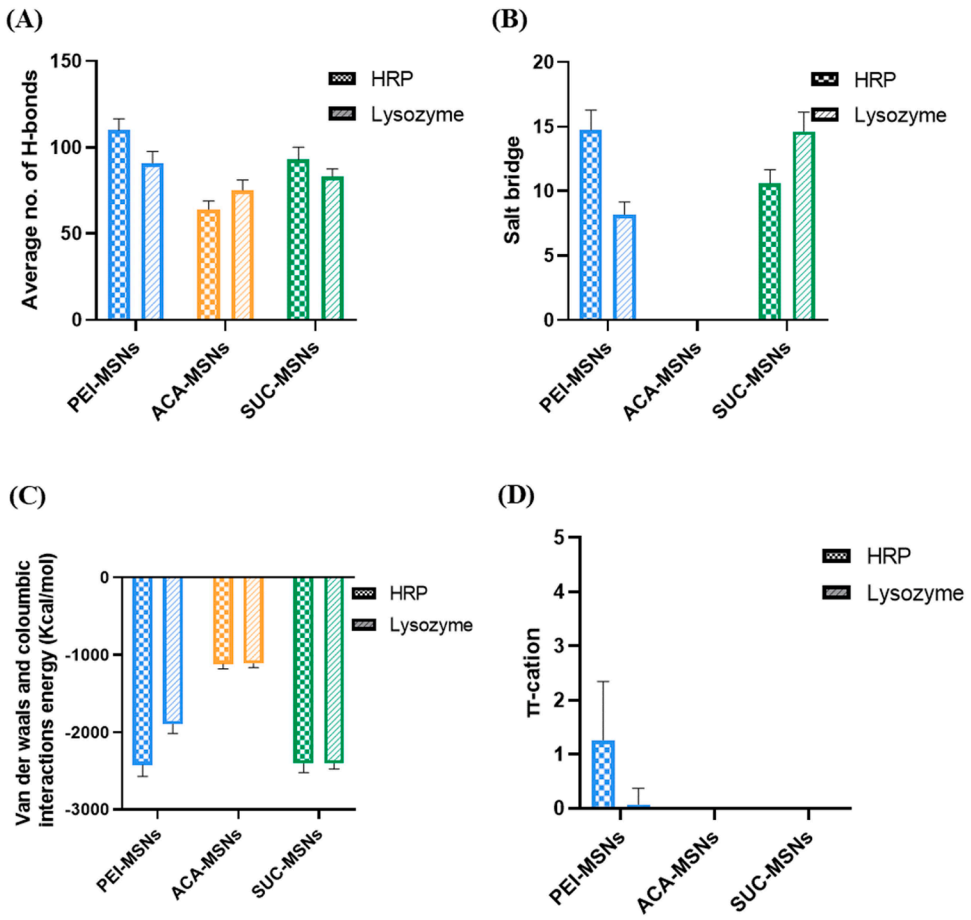

Fig. 6. Average of number of (A) hydrogen bonds, (B) salt bridges, (C) van der Waals and coulombic interactions energy and (D) π-cation interactions observed between surface modified MSNs and protein molecules during 100 ns long MD simulation.

both enzymes is similar in terms of the number of hydrogen bonds and van der Waals interaction energy (Fig. 6). However, it shows a higher magnitude of electrostatic interaction with lysozyme as compared to HRP. **Fig. S5A and B** shows the detailed interaction pattern of SUC-MSNs with HRP and lysozyme. SUC-MSNs, like PEI-MSNs, also show strong interaction with amino acids close to the active site, which could implicate some effect on the activity of these enzymes.

When compared to both PEI-MSNs and SUC-MSNs, the interactions of ACA-MSNs mainly occurred through residual unmodified silanol groups and remaining PEI functional groups. The chemically neutral ACA-MSNs are not directly involved in hydrogen bonding or salt bridges, but they show weak van der Waals and other hydrophobic interactions as detailed in Fig. 6 **and S6**.

To conclude, charged particles **(**PEI-MSNs and SUC-MSNs) showed more interaction points with both enzymes compared to ACA-MSNs. Regarding HRP, PEI-MSNs showed a higher number of interactions compared to others. On the other hand, SUC-MSNs showed more electrostatic interaction with lysozyme compared to PEI-MSNs. It was observed that capping the primary amino groups with the acetyl group (ACA-MSNs) showed less interaction with HRP and lysozyme (only hydrogen bonding and van der Waals).

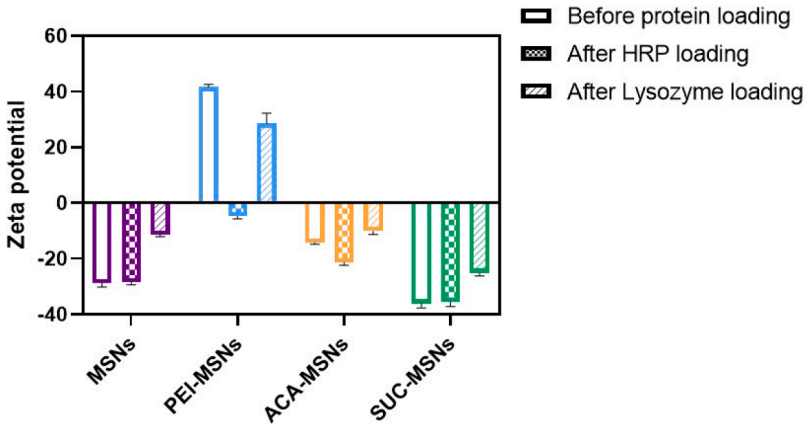

Fig. 7. ζ-potential of the surface-functionalized MSNs before and after enzyme immobilization (HRP and lysozyme) in HEPES buffer (pH 7.2, 25 mM).

4.4.2. ζ-potential of enzyme-immobilized MSN

Insights about protein adsorption on the net surface charge of the particles were obtained by measuring the ζ-potential of enzyme-loaded MSNs at neutral pH 7.4. Fig. 7 demonstrates the ζ-potential of the functionalized particles before and after protein adsorption. It was observed that loading of the negatively charged enzyme (HRP) lead to a significant change in the ζ-potential of positively charged MSNs (PEI-MSNs). The ζ-potential shifted from highly positive (+40 mV) to neutral or slightly negative (−4 mV), indicating strong interaction and screening of positively charged amino groups. Additionally, the net surface charge of near-neutral MSNs (ACA-MSNs) became more negative, shifting from −14 mV to −21 mV. In contrast, plain MSNs and negatively charged MSNs (SUC-MSNs) exhibited only a slight variation in their ζ-potential (1–2 mV). This can be explained by the high surface negativity of HRP, compensating for the charge reduction caused by the enzyme (Meder et al., 2012).

Conversely, lysozyme adsorption resulted in a decrease in the ζ-potential for all tested nanoparticles. The ζ-potential of plain MSNs and PEI-MSNs dropped to −11 mV and +28 mV, respectively. The net surface charge of near-neutral MSNs (ACA-MSNs) decreased to −10 mV, while the ζ-potential of the negatively charged particles (SUC-MSNs) shifted from −36 to −25 mV.

These results imply that enzyme adsorption onto different surface-functionalized MSNs modified the surface properties of the nanoparticle, making enzyme surface properties dominant and controlling the charge of the entire system (Meder et al., 2012; Dyawanapelly et al., 2019).

4.5. Biological activity of immobilized and free enzymes after release (specific activity and residual activity)

The main aim of any delivery system is to deliver functional protein to the target site. However, the interaction of proteins with nanoparticles can lead to changes in their sensitive structural confirmation. This is particularly crucial to consider when delivering enzymes, which may result in a reduction or total loss in their catalytic activity upon interaction with surfaces (Lin et al., 2011; Yiu and Wright, 2005). Generally, enzyme immobilization causes a decrease in enzyme activity relative to the free enzyme due to the physical interactions involved, which probably affects the accessibility of the active site of the enzymes (Gößl et al., 2019). Nevertheless, the degree of activity decrease is mainly dependent on the nanoparticle surface properties and the interaction closeness to the active site. Thus, measuring the enzymatic activity is a critical parameter to be considered not only after immobilization but also after free release from the carrier.

In the MD simulation, possible interactions involved between the model enzymes and different functionalized MSNs were presented. Here, the enzymatic activities of immobilized and free-released enzymes were evaluated to report the effect of these interactions on the functionality of the loaded enzymes. We measured the specific activity and residual activity of both enzymes (Fig. 8). In the residual activity, two different time points (24 h and 7 days) were chosen to cover the enzymatic activity during the release study. The catalytic activity of HRP-immobilized silica nanomaterials and free-released enzymes was measured following a standard activity assay based on the oxidation of TMB, while lysozyme activity was evaluated based on the change in the turbidity of a bacterial suspension (see materials and methods section). All activity data are compared to plain MSNs to exclude the effect of pore size and immobilization process and detect only the influence of the surface charge of the particles. It is worth noting that HRP is more sensitive to immobilization and showed a significant decrease in catalytic activity compared to lysozyme.

From Fig. 8**A and B**, it was observed that HRP immobilized onto positively charged MSNs (PEI-MSNs) showed a complete loss in activity compared to HRP immobilized onto ACA-MSNs (4 U/mg) and SUC-MSNs (1.5 U/mg). Regarding the residual activity, HRP released from PEI-MSNs exhibited no activity. HRP released from SUC-MSNs showed a decrease in activity to 19 % after 24 h and continuously decreased to 5 %

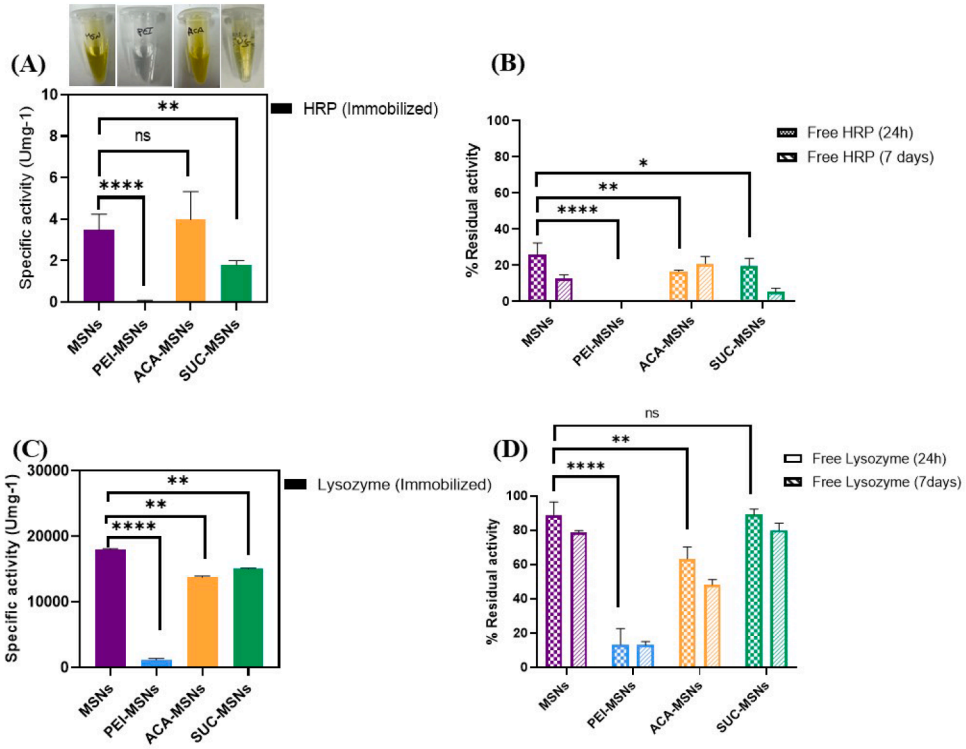

Fig. 8. Enzymatic activity of (A) immobilized HRP, (B) free released HRP, (C) immobilized lysozyme and (D) free released lysozyme. The residual activities refer to the free untreated enzymes. Data were presented as mean value ± SD ($n = 3$). Statistical differences between samples were analyzed using one-way ANOVA followed by Tukey's post-hoc test, with significance levels set at $^{*}p < 0.05$, $^{**}p < 0.01$, $^{***}p < 0.001$ and **** $p < 0.0001$.

after 7 days. The decrease in the enzyme activity after release can be explained by the low stability of the enzyme in the release medium. Interestingly, the activity of HRP released from ACA-MSNs decreased to 16 % after 24 h with no significant decrease after 7 days, indicating continuous release of active enzymes (Gaspar et al., 1998).

It was observed from Fig. 8**C and D** that the specific activity of lysozyme immobilized onto silica materials is 12 U/mg for PEI-MSNs, 13.5 $\times$ 10^3 U/mg for ACA-MSNs, and 15 $\times$ 10^3 U/mg for SUC-MSNs, respectively. On the other hand, the residual activity of lysozyme released from PEI-MSNs dramatically dropped to 13 % after 24 h with no significant change after 7 days. Moreover, lysozyme released from ACA-MSNs and SUC-MSNs exhibited activity of approximately 63 % and 89 % after 24 h, and 48 % and 80 % after 7 days, respectively.

From previous results, compared to MSNs, positively charged nanoparticles (PEI-MSNs) resulted in a complete loss of HRP activity (immobilized & free) and a substantial decrease in lysozyme activity (immobilized & free). A significant decrease in the enzyme activity observed with PEI-MSNs could be explained by the strong physical interactions observed between the PEI surfaces and acidic amino acid residues near the catalytic active site (Fig. 5). In HRP, this interaction near the active site might block the substrate diffusion, while in lysozyme, these acidic amino acids are crucial for the catalytic activity. Additionally, these interactions resulted in a significant alteration in the enzyme conformational structure, resulting in negligible activity observed in the free-released enzymes. Previous research conducted by Huang et al., (Huang et al., 2018) investigated the effect of hyperbranched PEI with different molecular weights on HRP activity. They confirmed significant structural changes in HRP structure, which was more significant with high molecular weight PEI. Additionally, the effect of PEI on enzyme inactivation was reported to be more significant if the polymer interacts with critical cations located in the internal pockets of proteins (Virgen-Ortiz et al., 2017).

In both enzymes, negatively charged MSNs (SUC-MSNs) reduced the activity of immobilized enzymes with less effect on the free enzymes. This decrease in the activity might be correlated to interaction with the basic amino acids near the enzyme's active site (**Fig. S5**). Although these interactions hinder the catalytic activity of the immobilized enzyme, it showed no significant effect on the released enzymes. While near-neutral nanoparticles (ACA-MSNs) showed no effect on HRP activity (immobilized), they showed a slight decrease in free HRP activity and lysozyme activity (immobilized & free). Near-neutral charged MSNs (ACA-MSNs) showed the least alteration in the enzyme activity with both enzymes, which might be attributed to the least interactions observed with the enzymes (**Fig. S6**). From Fig. 8**,** HRP-immobilized ACA-MSNs and lysozyme-immobilized SUC-MSNs showed the highest activity compared to others, whether released or immobilized on the

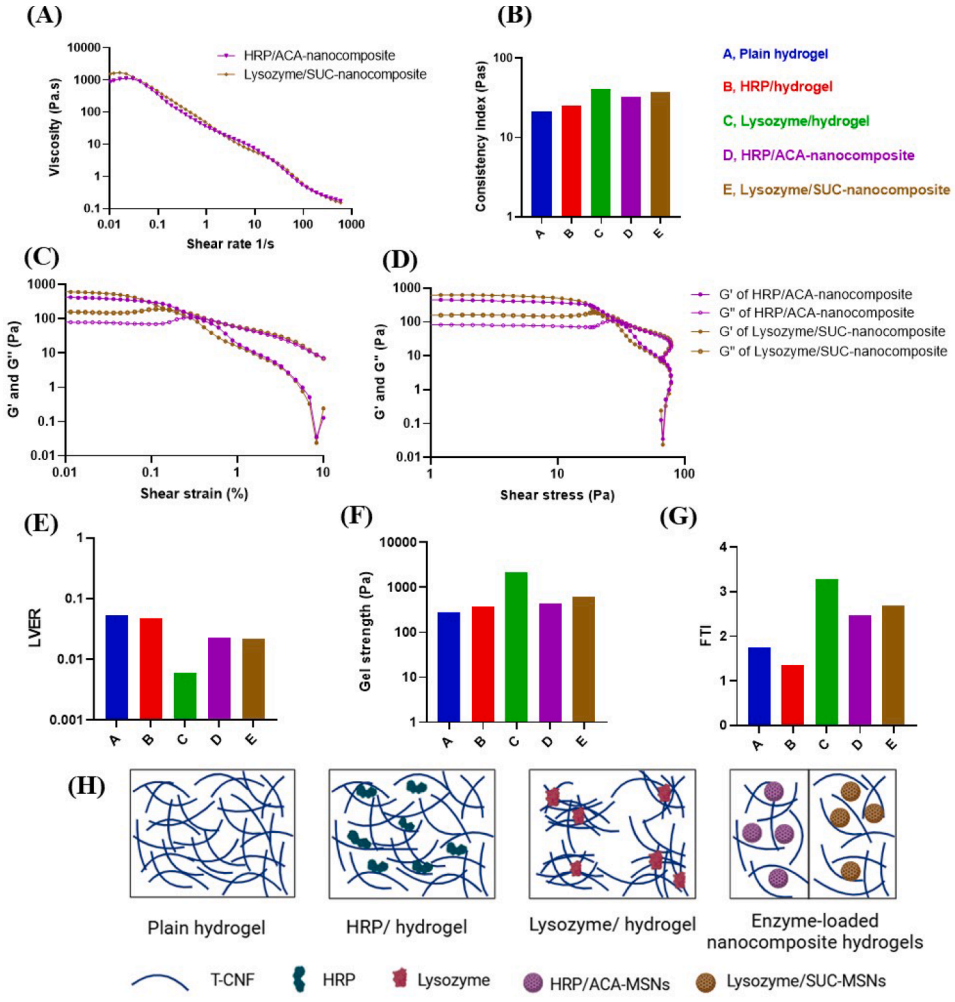

Fig. 9. Rheological properties of the prepared hydrogels (A) flow behavior and (B) consistency index. Amplitude sweep test as a function of (C) shear strain, (D) and shear stress. (E) The linear viscoelastic region (LVER), (F) gel strength, and (G) flow transition index (FTI). (H) Structural changes of T-CNF upon mixing with different surface-charged surfaces. Plain hydrogel showed fiber repulsion and fibril-fibril entanglement. HRP inserted between the fibers results in a decrease in fiber entanglement with no effect on fiber repulsion. Lysozyme adsorbed onto the fiber's surface results in a decrease in fiber repulsion with an increase in fiber aggregation. Enzyme-loaded nanoparticles inserted between the fibers result in decrease in fiber entanglement with no effect on fiber repulsion.

nanoparticles.

Based on the biological activity data, positively charged nanoparticles (PEI-MSNs) are excluded from the next study. Compared to all tested particles, ACA-MSNs were chosen as suitable carriers for the HRP with moderated adsorption capacity while maintaining optimal enzymatic activity. On the other hand, SUC-MSNs were selected for lysozyme loading due to their highest adsorption capacity and superior enzymatic activity.

4.6. Printing of the enzyme-loaded mesoporous silica nanocomposite hydrogel

4.6.1. Nanocomposite hydrogel preparation

To fabricate the biocatalytic nanocomposite hydrogel, HRP-loaded ACA-MSNs and lysozyme-loaded SUC-MSNs were physically incorporated into the polymeric matrix containing TEMPO-oxidized cellulose nanofibers (T-CNF), methacrylated galactoglucomannan (GGMMA), and lithium phenyl-2,4,6-trimethylbenzoylphosphinate (LAP). For comparison, free enzymes (HRP and lysozyme) without nanoparticles were mixed directly into the matrix as a reference sample.

4.6.2. Rheological assessment

Evaluation of the rheological properties of any developed hydrogel is considered an essential tool for studying its inner microstructure and stability (Hassan et al., 2019). It provides valuable information about flow behavior, viscosity, and viscoelasticity, all of which directly influence the efficiency of the 3D printing process of the developed ink. In our hydrogel, T-CNF serves as the main structural component, managing the rheological properties of the whole system. The stability and homogeneity of the T-CNF originate from the fibril-fibril entanglement and high electrostatic repulsion of the negatively charged carboxylate groups between the nanofibrils. Thus, incorporating charged surfaces may positively or negatively impact fiber repulsion. Based on the data obtained from our previous research, T-CNF is sensitive to positively charged nanoparticles. Nevertheless, the net surface charge of the chosen enzyme-loaded MSNs is compatible with T-CNF and suitable for the nanocomposite hydrogel preparation (Fig. 7).

The rheological properties of the tested formulations are illustrated in Fig. 9 **and Fig. S7**. As can be seen from Fig. 9**A and Fig. S7A**, the apparent viscosity of all formulations decreased along with increasing the shear rate, which indicates shear thinning behavior. This flow behavior is favorable for biomaterials intended for semi-solid extrusion 3D printing. For quantitative insights into the viscosity, the consistency index was calculated as the viscosity values at shear rate $1s^{-1}$ and compared in Fig. 9**B** It was observed that the lysozyme-hydrogel exhibits the highest consistency index value (41 Pas) compared to others. HRP-ACA-nanocomposite and lysozyme-SUC-nanocomposite showed a consistency index of 32 and 37 Pas, respectively. Both plain hydrogel and HRP-hydrogel showed the least consistency index value of 20 and 25 Pas, respectively. The increase in the consistency index with the lysozyme and nanoparticles indicates a change in the internal structure of the matrix compared to HRP. To detect these changes, the amplitude sweep test was conducted.

From the amplitude sweep test, viscoelastic moduli (storage modulus (G') and loss modulus (G'')) are presented as a function of shear strain and shear stress (Fig. 9**C and D**) and (**Fig.S7B and C**). For all tested samples, the storage modulus was higher than the loss modulus, indicating the elastic behavior of all samples. Different parameters were obtained, including linear viscoelastic region (LVER), gel strength, and flow transition index (FTI), and presented in Fig. 9**E-G**. LVER and gel strength indicate the hydrogel viscoelasticity, while FTI indicates the stress needed for the hydrogel to flow.

Compared to plain hydrogel, HRP-hydrogel showed less change in the matrix stability with an insignificant decrease in the LVER and FTI with a slight increase in the gel strength. This might be attributed to the negative net surface charge of HRP enhanced the repulsion between the negatively charged T-CNFs, which increased the gel strength. However, this increase in nanofibril repulsion resulted in a decrease in the fibril-fibril entanglement, which is responsible for the decrease in the FTI. On the other hand, lysozyme-hydrogel showed a significant decrease in the hydrogel LVER with increasing gel strength and FTI. Here, the increase in the gel strength can be explained by the adsorption behavior of the positively surface charged protein onto the negatively charged fibers, resulting in a decrease in the hydrogel colloidal stability by charge screening and increasing fibers aggregation. This aggregation leads to an increase in the stress needed for the hydrogel to flow. Prior findings reported by Wu et al., confirm the structural changes of T-CNF after lysozyme adsorption onto the fibers (Wu et al., 2021).

Both enzyme-loaded nanocomposites (HRP-ACA-nanocomposite hydrogel and lysozyme-SUC-nanocomposite hydrogel) showed the same behavior. Although the presence of nanoparticles enhanced the gel strength, it caused a slight decrease in the gel elasticity and an increase in the FTI. It was clear that the electrostatic attraction force between lysozyme and T-CNFs was shielded by immobilizing lysozyme into SUC-MSNs. Fig. 9**H** illustrates the structural changes of T-CNF upon mixing with different surface-charged surfaces.

4.7. Printing

Semi-solid 3D printing was selected as the scaffold fabrication technique, which depends significantly on the ink viscosity and viscoelastic properties. To translate the rheological behavior of the tested samples into practical outcomes, the printability of HRP-hydrogel, lysozyme-hydrogel, HRP-ACA-nanocomposite, and lysozyme-SUC-nanocomposite were tested. All tested formulations were successfully 3D printed except lysozyme-hydrogel (Fig. 10**A**). This might be attributed to what has been discussed earlier in the rheological assessment section 4.5.2. Screening of T-CNF charge by lysozyme adsorption results in fiber aggregation and thus hinders its printability. There was a negligible difference in the printability between HRP-ACA nanocomposite hydrogel and lysozyme-SUC-nanocomposite hydrogel.

Crosslinking of the printed scaffolds is a crucial step to retain the structure integrity of the printed scaffolds. The crosslinking degree regulates the mesh size of the polymeric network in the obtained hydrogels, which is implicative for the diffusion/release of the biological macromolecules and nanoparticle from the hydrogel matrix. Thus, all 3D printed constructs were photo-crosslinked using different UV post-curing times (1, 5, and 10 min). The effect of post-curing time on enzyme leaching and enzyme activity will be evaluated in the following sections.

4.7.1. Immobilization stability in the 3D printed structures

Here, the immobilization stability of the final formulations was evaluated by assessing the effect of two parameters on enzyme leaching: the hydrogel matrix and the UV post-curing time after the 3D printing process. From Fig. 10**B**, in all tested UV post-curing times, it was observed that HRP released from the 3D printed plain scaffolds showed burst release with about 45 % released within 1 hour. After 8 h, all samples reached a maximal percentage (60 % leached for 1 min post-curing time and 50 % for 5 and 10 min post-curing time). Compared to free nanoparticles, HRP, and lysozyme leached from the 3D printed ACA and SUC-nanocomposite scaffolds showed more sustained release to reach a maximum of 23 % and 57 % after 24 h, respectively (Fig. 10**B and C**). Thus, the nanoparticle incorporation into the hydrogel matrix could maintain enzyme immobilization for a longer time and provide slower and continuous enzyme release. In all nanocomposite samples, the varied UV post-curing time had a negligible effect on the enzyme release. However, we inferred that the photo-crosslinking of GGMMA in the ink system was already completed within 1 min post curing.

4.7.2. Enzymatic activity after 3D printing

The activity of the free-released enzymes after leaching from the 3D

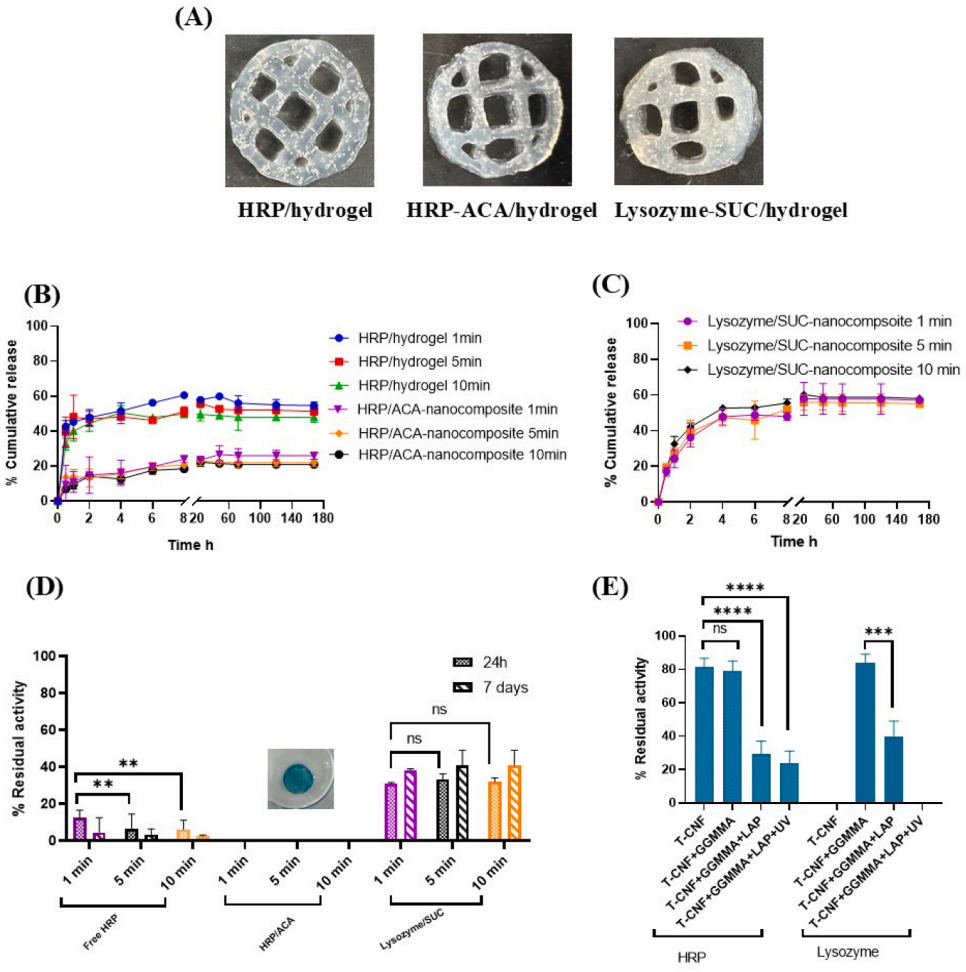

Fig. 10. (A) Photographic images of the 3D printed scaffolds. (B) Percent cumulative release of HRP from 3D printed plain constructs and ACA-nanocomposite and (C) percent cumulative release of lysozyme from 3D printed SUC-nanocomposite. (D) Percent residual activity of HRP and lysozyme after release from 3D printed scaffolds using different curing time (1, 5, 10 min) and (E) percent residual activity of free HRP and lysozyme after physical mixing with the hydrogel components and after exposure to UV light. The residual activities refer to the free untreated enzymes. Statistical differences between samples were analyzed using one-way ANOVA followed by Tukey's post-hoc test, with significance levels set at $^{**}p < 0.01$, $^{***}p < 0.001$ and **** $p < 0.0001$.

printed scaffolds was evaluated by measuring the activity after two different time points (24 h and 7 days) and compared with the enzyme activity before 3D printing. Clearly, both enzymes showed a significant decrease in activity after release from the 3D printed constructs. As seen in Fig. 10**D,** HRP released from the plain hydrogel scaffolds exposed to 1 min UV post-curing showed a significant decrease in the residual activity (12 % after 24 h). Additionally, their activity showed a decrease to 6 % after 5 and 10 min of UV post-curing. Further, it was clear that the activity of HRP significantly decreased after 7 days. In all tested UV post-curing times, HRP released from ACA-nanocomposite scaffolds showed a complete loss of enzyme activity. However, the activity of the immobilized HRP still could be detected within the nanocomposite scaffold. Similarly, lysozyme released from SUC-nanocomposite scaffolds showed a 60 % decrease in activity with an insignificant effect of the UV post-curing time. It is worth mentioning that the enzyme activity after 7 days showed no decrease, which indicates the continuous release of active enzymes with less effect of LAP on the enzymatic activity of the newly released enzyme.

The possible link between the hydrogel components and the reduction observed in enzyme activity was investigated by physically mixing HRP and lysozyme with the hydrogel components (T-CNF, GGMMA, and LAP with or without exposure to UV light) (Fig. 10**E).** Lysozyme activity could not be detected in the case of T-CNF and the matrix exposed to UV light due to assay limitations. It was observed that there is no significant difference between HRP activity detected with T-CNF alone or T-CNF and GGMMA, which indicates the negligible effect of GGMMA on the enzyme activity. HRP and lysozyme interaction with the hydrogel matrix (T-CNF and GGMMA) resulted in only a small decrease in enzyme activity (20 %). However, the presence of the photointiator (LAP) caused extensive inactivation of HRP and lysozyme (activity decreased by 70 % and 60 %, respectively). Exposing the HRP-hydrogel to UV light showed a slight decrease in the HRP activity compared to the untreated sample.

This reduction in enzyme activity results from the effect of free radicals on enzyme structure. LAP is a photointiator, which generates free radicals under the influence of applied light to initiate the photopolymerization of the hydrogels. It was reported that free radicals may induce conformational changes or fragmentation of the polypeptide chains. In enzymes, these modifications can lead to a complete loss of catalytic activity (Dumitru and Nechifor, 1994). From previous research, the presence of a photointiator was responsible for the reduction of β-galactosidase activity after the photopolymerization process (Suvarli et al., 2022). We concluded that LAP led to substantial inactivation of both enzymes, even in the absence of UV light, likely due to the generation of free radicals when exposed to daylight. Nevertheless, the reduction in activity is enzyme-specific. HRP is a peroxidase enzyme, which is more sensitive to the effect of free radicals than lysozyme.

4.8. Future remarks

Our study demonstrates the feasibility of delivering functional proteins with distinct properties using mesoporous silica nanocomposite biomaterials, highlighting both the potential advantages and limitations of the approach. A key consideration of utilizing enzymes in this study is ensuring their activity is retained after formulation, i.e. immobilization, hydrogel preparation and 3D printing in this case. Near-neutral MSNs are particularly useful for immobilizing sensitive negatively charged biologicals compared to the positively charged particles. This nanocomposite hydrogel supports diverse crosslinking methods post-3D printing. However, the photoinitiator negatively affected enzyme activity. This effect is critical if photo-crosslinking is used as the stabilizing method for the 3D printed constructs. Alternative crosslinking strategies other than photo-crosslinking may be preferred to eliminate the harm for photoinitiators.

Future research could explore the delivery of important biologicals, such as growth factors, to broaden the application of the developed nanocomposite hydrogel in tissue engineering. However, the release profile of the nanocomposite scaffold should be optimized to achieve a more sustained release over an extended period, thereby enhancing therapeutic efficacy. Additionally, both neutral and negatively charged MSNs facilitate the delivery and semi-solid 3D printing of positively charged biomolecules in combination with anionic cellulose nanofibers.

5. Conclusions

We have successfully fabricated 3D printed biocatalytic scaffolds composed of mesoporous silica nanocomposite hydrogels, suitable for immobilizing enzymes with distinct properties (different sizes and isoelectric points). Two model enzymes, HRP and lysozyme, were immobilized into MSNs with different surface charges. The adsorption capacity (immobilization and immobilization stability) and the biological activity of the immobilized enzymes were evaluated. To investigate potential interactions between the enzymes and differently surface-charged MSNs, we conducted two independent studies utilizing MP-SPR and MD simulations. Both methods complemented our initial observation where positively charged nanoparticles (PEI-MSNs) showed the highest adsorption capacity for HRP but also resulted in a complete loss of the HRP activity and a substantial reduction of the lysozyme activity. In contrast, negatively charged MSNs (SUC-MSNs) displayed the highest adsorption capacity while retaining the catalytic activity of lysozyme compared to PEI-MSNs. Near-neutral MSNs (ACA-MSNs) demonstrated moderate adsorption with minimal effect on the catalytic activity of both enzymes. As a result, HRP-loaded ACA-MSNs and lysozyme-loaded SUC-MSNs were identified as the optimal choices for nanocomposite fabrication. These were subsequently incorporated into a plant-based and photocrosslinkable hydrogel consisting of T-CNF and GGMMA and compared with enzyme-loaded hydrogels. All formulations, except the lysozyme-loaded hydrogels, were successfully 3D printed. Although enzymes leached from the 3D nanocomposite scaffolds demonstrate more sustained release compared to hydrogel-loaded enzymes without nanoparticles, their catalytic activity was significantly reduced in the presence of photoinitiator (LAP). In conclusion, the net surface charge of the integrated nanoparticles plays a pivotal role in controlling immobilization stability and preserving biological activity. While oppositely charged surfaces offer high adsorption capacity, they may compromise the biological activity of the loaded proteins. The flexibility of the fabricated MSN-laden nanocomposite biomaterial enables the delivery of various biologicals with high immobilization stability and acceptable biological activity.

Data availability statement

The data that support the findings of this study are available in the supplementary material of this article.

CRediT authorship contribution statement

Alaa Mahran: Writing – original draft, Visualization, Validation, Methodology, Investigation, Formal analysis, Conceptualization. **Fadak Howaili:** Writing – original draft, Visualization, Validation, Methodology, Investigation, Formal analysis, Conceptualization. **Rajendra Bhadane:** Writing – original draft, Visualization, Validation, Methodology, Investigation, Formal analysis, Conceptualization. **Rathna Mathiyalagan:** Writing – review & editing, Validation. **Tapani Viitala:** Writing – review & editing, Supervision, Resources, Conceptualization. **Xiaoju Wang:** Writing – review & editing, Supervision, Resources, Funding acquisition, Conceptualization. **Jessica M. Rosenholm:** Writing – review & editing, Supervision, Resources, Project administration, Funding acquisition, Conceptualization.

Declaration of competing interest

The authors declare no conflicts of interest.

Acknowledgments

Transmission electron microscopy samples were performed at the Electron Microscopy Laboratory, Institute of Biomedicine, University of Turku, and Biocenter Finland. A. Mahran would like to acknowledge the financial support from the Ministry of Higher Education of the Arab Republic of Egypt. X. Wang would like to thank the Research Council of Finland for the Academy Research Fellow project (333158) for her research at ÅAU. The Business Finland co-innovation project “3D Cure” (575/31/2023), PoDoCo, and Swedish cultural foundation (grant number 190913) are acknowledged for funding support. R. Mathiyalagan greatly acknowledges the Åbo Akademi University doctoral research grant and Finnish Pharmaceutical Society research grant. Dhayakumar Rajan Prakash and Tomi Kalpio from Brinter AM Technologies Ltd (Turku, Finland) are acknowledged for kind support to technical perspectives of operating the Brinter ONE 3D BioPrinter. This research is also aligned with the strategic research profiling area “Solutions for Health” at Åbo Akademi University (funded by the Research Council/Academy of Finland, 336355) and parts of the research used the Research Council of Finland Research Infrastructure “Printed Intelligence Infrastructure” (PII-FIRI). R. Bhadane wish to acknowledge CSC–IT Center for Science, Finland, for generous computational resources.

Supplementary materials

Supplementary material associated with this article can be found, in the online version, at doi:10.1016/j.ejps.2025.107132.

Data availability

Data will be made available on request.

References

Berglund, Gunnar I., Carlsson, Gunilla H., Smith, Andrew T., Szöke, Hanna, Henriksen, Anette, Hajdu, Janos, 2002. The catalytic pathway of horseradish peroxidase at high resolution. Nature 417, 463–468.

Berman, Helen M., Westbrook, John, Feng, Zukang, Gilliland, Gary, Bhat, T.N., Weissig, Helge, Shindyalov, Ilya N., Bourne, Philip E., 2000. The Protein Data Bank. Nucleic. Acids. Res. 28, 235–242.

Bowers, Kevin J, Albright, Brian James, Yin, Lilan, Bergen, B., Kwan, Thomas JT, 2008. Ultrahigh performance three-dimensional electromagnetic relativistic kinetic plasma simulation. Phys. Plasmas. 15.

Braga, Carlos, Travis, Karl P, 2005. A configurational temperature Nosé-Hoover thermostat. J. Chem. Phys. 123.

Castillo, Rafael R, Lozano, Daniel, Vallet-Regí, María, 2020. Mesoporous silica nanoparticles as carriers for therapeutic biomolecules. Pharmaceutics. 12, 432.

Chakraborty, Aishik, Roy, Avinava, Ravi, Shruthi Polla, Paul, Arghya, 2021. Exploiting the role of nanoparticles for use in hydrogel-based bioprinting applications: concept, design, and recent advances. Biomater. Sci. 9, 6337–6354.
Chen, Gong, Tang, Wenwei, Wang, Xiaohui, Zhao, Xueling, Chen, Cheng, Zhu, Zhigang, 2019. Applications of hydrogels with special physical properties in biomedicine. Polymers. (Basel) 11, 1420.
Chernozem, Roman V, Surmeneva, Maria A, Abalymov, Anatolii A, Parakhonskiy, Bogdan V, Rigole, Petra, Coenye, Tom, Surmenev, Roman A, Skirtach, Andre G, 2021. Piezoelectric hybrid scaffolds mineralized with calcium carbonate for tissue engineering: analysis of local enzyme and small-molecule drug delivery, cell response and antibacterial performance. Materials Science and Engineering: C 122, 111909.
Chouyyok, Wilaiwan, Panpranot, Joongjai, Thanachayanant, Chanchana, Prichanont, Seeroong, 2009. Effects of pH and pore characters of mesoporous silicas on horseradish peroxidase immobilization. Journal of Molecular Catalysis B: Enzymatic 56, 246–252.
Deere, Joseph, Magner, Edmond, Gerard Wall, J., Kieran Hodnett, B., 2002. Mechanistic and structural features of protein adsorption onto mesoporous silicates. The Journal of Physical Chemistry B 106, 7340–7347.
Dumitru, Ioan Florea, Nechifor, Marina Tamara, 1994. Decrease in yeast glucose-6-phosphate dehydrogenase activity due to oxygen free radicals. Int. J. Biochem. 26, 229–233.
Dyawanapelly, Sathish, Mehrotra, Pihu, Ghosh, Goutam, Jagtap, Dhanashree D, Dandekar, Prajakta, Jain, Ratnesh, 2019. How the surface functionalized nanoparticles affect conformation and activity of proteins: exploring through protein-nanoparticle interactions. Bioorg. Chem. 82, 17–25.
Gaspar, Maria Manuela, Blanco, Dolores, Cruz, Maria Eugenia M, Alonso, Maria Jose, 1998. Formulation of L-asparaginase-loaded poly (lactide-co-glycolide) nanoparticles: influence of polymer properties on enzyme loading, activity and in vitro release. Journal of controlled release 52, 53–62.
GhavamiNejad, Amin, Ashammakhi, Nureddin, Wu, Xiao Yu, Khademhosseini, Ali, 2020. Crosslinking strategies for 3D bioprinting of polymeric hydrogels. Small. 16, 2002931.
Gößl, Dorothée, Singer, Helena, Chiu, Hsin-Yi, Schmidt, Alexandra, Lichtnecker, Martina, Engelke, Hanna, Bein, Thomas, 2019. Highly active enzymes immobilized in large pore colloidal mesoporous silica nanoparticles. New Journal of Chemistry 43, 1671–1680.
Hassan, Mahbub, Dave, Khyati, Chandrawati, Rona, Dehghani, Fariba, Gomes, Vincent G, 2019. 3D printing of biopolymer nanocomposites for tissue engineering: nanomaterials, processing and structure-function relation. Eur. Polym. J. 121, 109340.
Hickey, Ryan J, Pelling, Andrew E, 2019. Cellulose biomaterials for tissue engineering. Front. Bioeng. Biotechnol. 7, 45.
Holliday, Gemma L, Mitchell, John BO, Thornton, Janet M, 2009. Understanding the functional roles of amino acid residues in enzyme catalysis. J. Mol. Biol. 390, 560–577.
Hölzl, Katja, Lin, Shengmao, Tytgat, Liesbeth, Van Vlierberghe, Sandra, Gu, Linxia, Ovsianikov, Aleksandr, 2016. Bioink properties before, during and after 3D bioprinting. Biofabrication. 8, 032002.
Hoover, William G., 1985. Canonical dynamics: equilibrium phase-space distributions. Physical review A 31, 1695.
Huang, Aimin, Wei, Bangzhi, Mo, Junyong, Wang, Yajing, Ma, Lin, 2018. Conformation and activity alteration of horseradish peroxidase induced by the interaction with gene carrier polyethyleneimines. Spectrochimica Acta Part A: Molecular and Biomolecular Spectroscopy 188, 90–98.
Kao, Kun-Che, Lin, Tien-Sung, Mou, Chung-Yuan, 2014. Enhanced activity and stability of lysozyme by immobilization in the matching nanochannels of mesoporous silica nanoparticles. The Journal of Physical Chemistry C 118, 6734–6743.
Karaman, Didem Sen, Desai, Diti, Senthilkumar, Rajendran, Johansson, Emma M, Råtts, Natalie, Odén, Magnus, Eriksson, John E, Sahlgren, Cecilia, Toivola, Diana M, Rosenholm, Jessica M, 2012. Shape engineering vs organic modification of inorganic nanoparticles as a tool for enhancing cellular internalization. Nanoscale Res. Lett. 7, 1–14.
Koretz, Kirsten S, McGraw, Claire E, Stradley, Steven, Elbaradei, Ahmed, Malmstadt, Noah, Robinson, Anne S, 2021. Characterization of binding kinetics of A2AR to Gαs protein by surface plasmon resonance. Biophys. J. 120, 1641–1649.
Kubiak-Ossowska, Karina, Jachimska, Barbara, Al Qaraghuli, Mohammed, Mulheran, Paul A, 2019. Protein interactions with negatively charged inorganic surfaces. Curr. Opin. Colloid. Interface Sci. 41, 104–117.
Lin, Na, Gao, Ling, Chen, Zhe, Zhu, Jian Hua, 2011. Elevating enzyme activity through the immobilization of horseradish peroxidase onto periodic mesoporous organosilicas. New Journal of Chemistry 35, 1867–1875.
Lu, Chao, Wu, Chuanjie, Ghoreishi, Delaram, Chen, Wei, Wang, Lingle, Damm, Wolfgang, Ross, Gregory A, Dahlgren, Markus K, Russell, Ellery, Bargen, Christopher D Von, 2021. OPLS4: improving force field accuracy on challenging regimes of chemical space. J. Chem. Theory. Comput. 17, 4291–4300.
Mahran, Alaa, Özliseli, Ezgi, Wang, Qingbo, Özliseli, Ilayda, Bhadane, Rajendra, Xu, Chunlin, Wang, Xiaoju, Rosenholm, Jessica M, 2023. Semi-solid 3D printing of mesoporous silica nanoparticle-incorporated xeno-free nanomaterial hydrogels for protein delivery. Nano Select 4, 598–614.
Martyna, Glenn J, Hughes, Adam, Tuckerman, Mark E, 1999. Molecular dynamics algorithms for path integrals at constant pressure. J. Chem. Phys. 110, 3275–3290.
Meder, Fabian, Daberkow, Timo, Treccani, Laura, Wilhelm, Michaela, Schowalter, Marco, Rosenauer, Andreas, Mädler, Lutz, Rezwan, Kurosch, 2012. Protein adsorption on colloidal alumina particles functionalized with amino, carboxyl, sulfonate and phosphate groups. Acta Biomater. 8, 1221–1229.
Merlini, Giampaolo, Bellotti, Vittorio, 2005. Lysozyme: a paradigmatic molecule for the investigation of protein structure, function and misfolding. Clinica chimica acta 357, 168–172.
Miyahara, Masahiko, Vinu, Ajayan, Zakir Hossain, Kazi, Nakanishi, Takashi, Ariga, Katsuhiko, 2006. Adsorption study of heme proteins on SBA-15 mesoporous silica with pore-filling models. Thin. Solid. Films. 499, 13–18.
Monavari, Mahshid, Medhekar, Rucha, Nawaz, Qaisar, Monavari, Mehran, Fuentes-Chandía, Miguel, Homaeigohar, Shahin, Boccaccini, Aldo R, 2022. A 3D Printed Bone Tissue Engineering Scaffold Composed of Alginate Dialdehyde-Gelatine Reinforced by Lysozyme Loaded Cerium Doped Mesoporous Silica-Calcia Nanoparticles. Macromol. Biosci. 22, 2200113.
Olsson, Mats HM, Søndergaard, Chresten R, Rostkowski, Michal, Jensen, Jan H, 2011. PROPKA3: consistent treatment of internal and surface residues in empirical p K a predictions. J. Chem. Theory. Comput. 7, 525–537.
Özliseli, Ezgi, Şanlıdağ, Sami, Süren, Behice, Mahran, Alaa, Parikainen, Marjaana, Sahlgren, Cecilia, Rosenholm, Jessica M, 2023. Directing cellular responses in a nanocomposite 3D matrix for tissue regeneration with nanoparticle-mediated drug delivery. Mater. Today Bio 23, 100865.
Pandey, Veda P, Awasthi, Manika, Singh, Swati, Tiwari, Sameeksha, Dwivedi, Upendra N, 2017. A comprehensive review on function and application of plant peroxidases. Biochem. Anal. Biochem. 6, 308.
Popat, Amirali, Hartono, Sandy Budi, Stahr, Frances, Liu, Jian, Qiao, Shi Zhang, Lu, Gao Qing Max, 2011. Mesoporous silica nanoparticles for bioadsorption, enzyme immobilisation, and delivery carriers. Nanoscale 3, 2801–2818.
Pota, Giulio, Salerno, Antonio Sapienza, Costantini, Aniello, Silvestri, Brigida, Passaro, Jessica, Califano, Valeria, 2022. Co-immobilization of cellulase and β-glucosidase into mesoporous silica nanoparticles for the hydrolysis of cellulose extracted from Eriobotrya japonica Leaves. Langmuir. 38, 5481–5493.
Predescu, Cristian, Lerer, Adam K, Lippert, Ross A, Towles, Brian, Grossman, J.P., Dirks, Robert M, Shaw, David E, 2020. The u-series: a separable decomposition for electrostatics computation with improved accuracy. J. Chem. Phys. 152.
Rahmatika, Annie M, Goi, Yohsuke, Kitamura, Takeo, Widiyastuti, W., Ogi, Takashi, 2019. TEMPO-oxidized cellulose nanofiber (TOCN) decorated macroporous silica particles: synthesis, characterization, and their application in protein adsorption. Materials Science and Engineering: C 105, 110033.
Rezwan, Kurosch, Meier, Lorenz P, Gauckler, Ludwig J, 2005. Lysozyme and bovine serum albumin adsorption on uncoated silica and AlOOH-coated silica particles: the influence of positively and negatively charged oxide surface coatings. Biomaterials 26, 4351–4357.
Rosenholm, Jessica M., Lindén, Mika, 2007. Wet-Chemical Analysis of Surface Concentration of Accessible Groups on Different Amino-Functionalized Mesoporous SBA-15 Silicas. Chemistry of Materials 19, 5023–5034.
Sang, Lung-Ching, Vinu, Ajayan, Coppens, Marc-Olivier, 2011. General description of the adsorption of proteins at their iso-electric point in nanoporous materials. Langmuir. 27, 13828–13837.
Shelley, John C, Cholleti, Anuradha, Frye, Leah L, Greenwood, Jeremy R, Timlin, Mathew R, Uchimaya, Makoto, 2007. Epik: a software program for pK a prediction and protonation state generation for drug-like molecules. J. Comput. Aided. Mol. Des. 21, 681–691.
Shen, Dengke, Yang, Jianping, Li, Xiaomin, Zhou, Lei, Zhang, Renyuan, Li, Wei, Chen, Lei, Wang, Rui, Zhang, Fan, Zhao, Dongyuan, 2014. Biphase stratification approach to three-dimensional dendritic biodegradable mesoporous silica nanospheres. Nano Lett. 14, 923–932.
Shen, Xiaotong, Yang, Miao, Cui, Caixia, Cao, Hui, 2019. In situ immobilization of glucose oxidase and catalase in a hybrid interpenetrating polymer network by 3D bioprinting and its application. Colloids and Surfaces A: Physicochemical and Engineering Aspects 568, 411–418.
Bakhtiari, Soleymani Eil, Sanaz, Bakhsheshi-Rad, Hamid Reza, Karbasi, Saeed, Razzaghi, Mahmood, Tavakoli, Mohamadreza, Ismail, Ahmad Fauzi, Sharif, Safian, RamaKrishna, Seeram, Chen, Xiongbiao, Berto, Filippo, 2021. 3-dimensional printing of hydrogel-based nanocomposites: a comprehensive review on the technology description, properties, and applications. Adv. Eng. Mater. 23, 2100477.
Søndergaard, Chresten R, Olsson, Mats HM, Rostkowski, Michał, Jensen, Jan H, 2011. Improved treatment of ligands and coupling effects in empirical calculation and rationalization of p K a values. J. Chem. Theory. Comput. 7, 2284–2295.
Souto, Dênio EP, Fonseca, Aliani M, Barragan, José TC, Luz, Rita de CS, Andrade, Hélida M, Damos, Flávio S, Kubota, Lauro T, 2015. SPR analysis of the interaction between a recombinant protein of unknown function in Leishmania infantum immobilised on dendrimers and antibodies of the visceral leishmaniasis: a potential use in immunodiagnosis. Biosensors and Bioelectronics 70, 275–281.
Su, T.J., Green, R.J., Wang, Y., Murphy, E.F., Lu, J.R., Ivkov, R., Satija, S.K., 2000. Adsorption of lysozyme onto the silicon oxide surface chemically grafted with a monolayer of pentadecyl-1-ol. Langmuir. 16, 4999–5007.
Sufiyan, Mohd, Kushwaha, Poonam, Ahmad, Mohammad, Mandal, Purba, Vishwakarma, Km Khushbo, 2024. Scaffold-Mediated Drug Delivery for Enhanced Wound Healing: a Review. AAPS. PharmSciTech. 25, 137.
Suvarli, Narmin, Wenger, Lukas, Serra, Christophe, Perner-Nochta, Iris, Hubbuch, Jürgen, Wörner, Michael, 2022. Immobilization of β-Galactosidase by Encapsulation of Enzyme-Conjugated Polymer Nanoparticles Inside Hydrogel Microparticles. Front. Bioeng. Biotechnol. 9.
Tu, Jing, Boyle, Aimee L, Friedrich, Heiner, Bomans, Paul HH, Bussmann, Jeroen, Sommerdijk, Nico AJM, Jiskoot, Wim, Kros, Alexander, 2016. Mesoporous silica nanoparticles with large pores for the encapsulation and release of proteins. ACS. Appl. Mater. Interfaces. 8, 32211–32219.
Vashist, Arti, Ahmad, Sharif, 2015. Hydrogels in tissue engineering: scope and applications. Curr. Pharm. Biotechnol. 16, 606–620.

Veitch, Nigel C., 2004. Horseradish peroxidase: a modern view of a classic enzyme. Phytochemistry 65, 249–259.
Vinu, a A, Murugesan, V., Hartmann, Martin, 2004. Adsorption of lysozyme over mesoporous molecular sieves MCM-41 and SBA-15: influence of pH and aluminum incorporation. The Journal of Physical Chemistry B 108, 7323–7330.
Virgen-Ortiz, Jose J, Santos, José CS Dos, Berenguer-Murcia, Ángel, Barbosa, Oveimar, Rodrigues, Rafael C, Fernandez-Lafuente, Roberto, 2017. Polyethylenimine: a very useful ionic polymer in the design of immobilized enzyme biocatalysts. Journal of Materials Chemistry B 5, 7461–7490.
Wang, Qi, Luo, Zheng, Wu, Yun-Long, Li, Zibiao, 2023. Recent Advances in Enzyme-Based Biomaterials Toward Diabetic Wound Healing. Adv. Nanobiomed. Res. 3, 2200110.
Wang, Xia, Wang, Qigang, 2021. Enzyme-laden bioactive hydrogel for biocatalytic monitoring and regulation. Acc. Chem. Res. 54, 1274–1287.
Wang, Yajun, Caruso, Frank, 2005. Mesoporous silica spheres as supports for enzyme immobilization and encapsulation. Chemistry of Materials 17, 953–961.
Wang, Yue, Ahmad Nor, Yusilawati, Song, Hao, Yang, Yannan, Xu, Chun, Yu, Meihua, Yu, Chengzhong, 2016. Small-sized and large-pore dendritic mesoporous silica nanoparticles enhance antimicrobial enzyme delivery. Journal of Materials Chemistry B 4, 2646–2653.
Weishaupt, Ramon, Siqueira, Gilberto, Schubert, Mark, Tingaut, Philippe, Maniura-Weber, Katharina, Zimmermann, Tanja, Thöny-Meyer, Linda, Faccio, Greta, Ihssen, Julian, 2015. TEMPO-oxidized nanofibrillated cellulose as a high density carrier for bioactive molecules. Biomacromolecules. 16, 3640–3650.
Weiss, Manfred S, Palm, Gottfried J, Hilgenfeld, Rolf, 2000. Crystallization, structure solution and refinement of hen egg-white lysozyme at pH 8.0 in the presence of MPD. Acta Crystallographica Section D: Biological Crystallography 56, 952–958.
Wu, Tingting, Kummer, Nico, Kevin, J., Campioni, Silvia, Zeng, Zhihui, Siqueira, Gilberto, Dong, Jie, Nyström, Gustav, 2021. Nanocellulose-lysozyme colloidal gels via electrostatic complexation. Carbohydr. Polym. 251, 117021.
Xiao, Qing-Gui, Tao, Xia, Zou, Hai-Kui, Chen, Jian-Feng, 2008. Comparative study of solid silica nanoparticles and hollow silica nanoparticles for the immobilization of lysozyme. Chemical Engineering Journal 137, 38–44.
Yiu, Humphrey HP, Wright, Paul A, 2005. Enzymes supported on ordered mesoporous solids: a special case of an inorganic–organic hybrid'. J. Mater. Chem. 15, 3690–3700.
Zhou, Zhou, Hartmann, Martin, 2013. Progress in enzyme immobilization in ordered mesoporous materials and related applications. Chem. Soc. Rev. 42, 3894–3912.
Zielińska, Aleksandra, Karczewski, Jacek, Eder, Piotr, Kolanowski, Tomasz, Szalata, Milena, Wielgus, Karolina, Szalata, Marlena, Kim, Dohun, Shin, Su Ryon, Słomski, Ryszard, 2023. Scaffolds for drug delivery and tissue engineering: the role of genetics. Journal of Ophthalmology Clinics and Research 359, 207–223.